IOWA STATE UNIVERSITY
Digital Repository

1969

Applications of the induction coupled plasma to analytical spectroscopy

George Wilson Dickinson
Iowa State University

APPLICATIONS OF THE INDUCTION COUPLED PLASMA

TO ANALYTICAL SPECTROSCOPY

by

George Wilson Dickinson

A Dissertation Submitted to the

Graduate Faculty in Partial Fulfillment of

The Requirement for the Degree of

DOCTOR OF PHILOSOPHY

Major Subject: Analytical Chemistry

Approved:

In Charge of Major Work

Head of Major Department

Dean) of Graduate College

Iowa State University
Ames, Iowa

1969

TABLE OF CONTENTS

INTRODUCTION

A plasma is any gas in which a significant fraction of its atoms or molecules are ionized. A plasma is thus a good electrical conductor and, as such, may interact with electric and magnetic fields. The coupling of a plasma once formed, to a high frequency, alternating magnetic field provides a means of continually supplying the energy required to maintain the plasma.

In an induction-coupled plasma, an axial magnetic field is produced by a high frequency, alternating current flowing in a solenoid inductor surrounding the plasma volume. The alternating field accelerates the electrons in the plasma which transfer a portion of their kinetic energy to the atoms in the plasma upon collision. If this energy is sufficient, the atom may be excited or ionized. Ionization provides more electrons thereby perpetuating the plasma. Eddy currents are induced in azimuthal closed current paths within the plasma which meet resistance to their flow and Joule heating results. This process is analogous to the induction-heating of a metallic cylinder. The energy absorbed by the plasma is released in the form of heat and light when the dissociated particles recombine.

Since a gas is not a good conductor until it is ionized, a supply of electrons of sufficient energy to ionize the gas must be made available to initiate the plasma. Methods of initiation include low pressure breakdown (1) or formation of a pilot discharge in the plasma region to which the magnetic field can couple. Pilot discharges have been formed by auxiliary arcs (2) and tesla coil sparks (3). However, the simplest and most practical method of initiation, as first indicated by Reed (2), is the insertion of a refractory conducting rod such as graphite into the discharge region within the solenoid. The rod is inductively heated, thermal electrons are emitted and are accelerated by the magnetic field. These electrons ionize a portion of the gas next to the rod forming a small pilot plasma which couples to the magnetic field and instantly expands into the main plasma.

Historical Development

The first experiments with induction-coupled plasma generation were conducted by Babat (4) in the early 1940's. Babat described the electrical and magnetic properties, circuit requirements, and general appearance of both the capacitive and induction-coupled plasma at frequencies from 1 to 100 MHz, at pressures of one atmosphere and less, and at power levels up to 100 kw. He observed that the

power generated in the plasma at and near atmospheric pressure
was at the kilowatt level rather than the watt level character-
istic of low pressure plasmas. These investigations, however,
were carried out with a static system and no attempt was
made to develop applications for the plasma.

To prevent the plasma from contacting the solenoid
inductor and causing a short circuit, the plasma must be
contained by a dielectric material. Babat successfully
employed a quartz tube for containment of low pressure
plasmas. However, with atmospheric pressure plasmas at
the kilowatt power level, the quartz tube often melted and
the plasma was extinguished. Some means of thermally
isolating the plasma from the confining material was
evidently needed.

Plasma formation by inductive coupling was essentially
forgotten until the early 1960's when Reed (2,5) developed
the induction-coupled plasma into a torch like discharge.
Reed used a 4 MHz, 10 kw generator to form an atmospheric
pressure plasma with argon flowing through a one-inch
diameter quartz tube. The plasma thus formed resembles
the chemical flame in appearance. Reed's ingenious solution
to the thermal isolation problem was to introduce the argon
tangentially into the tube. The gas spiraled up the tube
wall, centering the plasma, stabilizing it, and cooling the
tube walls. Reed contended that tangential flow was necessary

at high flow rates to maintain the plasma since it resulted in some of the plasma gas being recirculated by vortex flow. A plasma with tangential gas introduction is termed a vortex flow stabilized plasma and is illustrated schematically in Figure 1A.

In a later torch design employed by Wendt and Fassel (6), the gas was introduced in a near laminar or coaxial flow pattern. The torch was a dual tube design with a high velocity gas flow through the outer tube which cooled the tube walls and stabilized the plasma. A low velocity gas flow through the center tube supplied the plasma support gas. A schematic diagram of the coaxial flow pattern is shown in Figure 1B. With this flow pattern the plasma was found easier to initiate and materials introduced into the plasma were not accelerated toward the confining tube walls as with vortex flow.

Reed's initial application for the induction-coupled plasma was for the growth of single crystals (7). Since then the plasma has been the subject of numerous investigations and applications which have been adequately reviewed by Wendt (8).

Application to Analytical Spectroscopy

Of particular interest to the analytical chemist is the potential applicability of the induction-coupled plasma to analytical spectroscopy. The flame-like plasma is a stable,
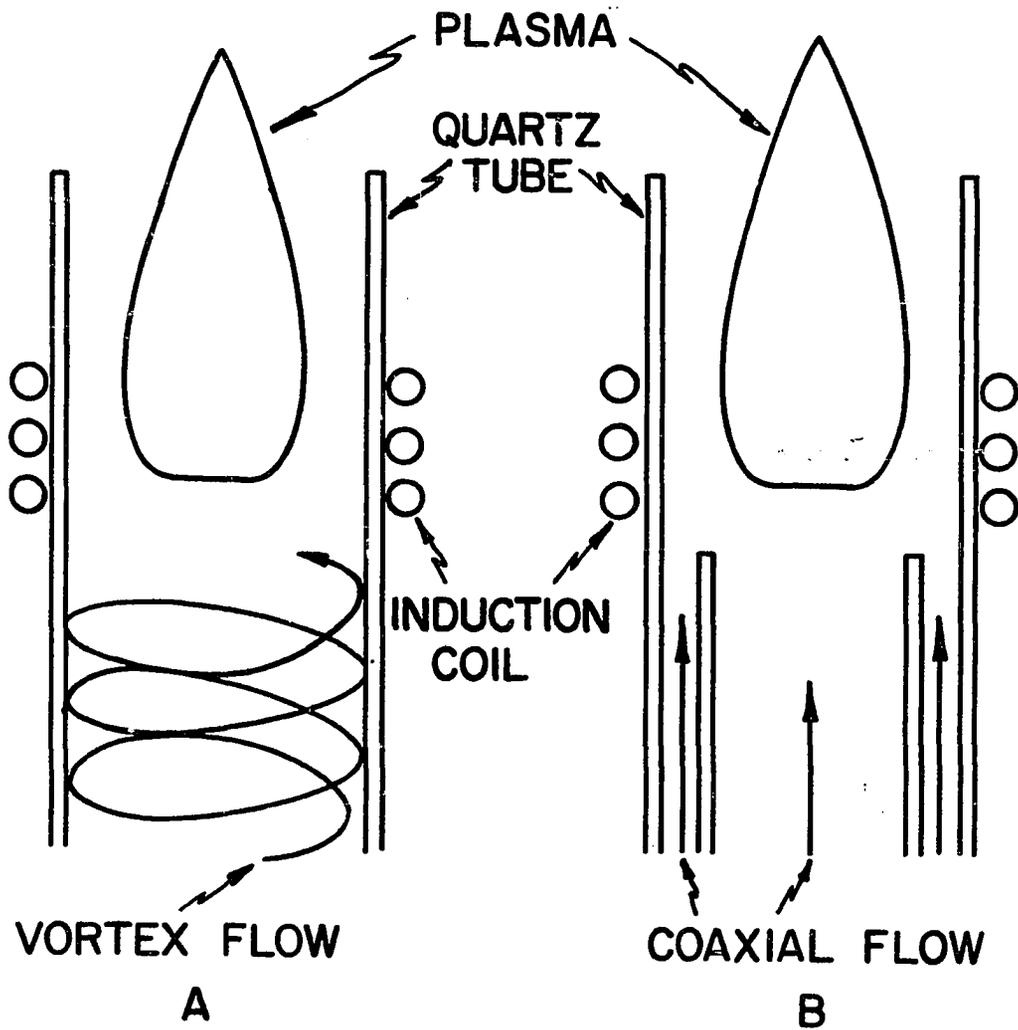
Figure 1. Two plasma torch gas flow patterns

high temperature source, free of contamination from electrodes.
Since any gas can, in principle, be used to maintain the plasma,
the environment presented to any material introduced can be
chemically controlled. These features and the ability to
introduce samples via the continuously flowing plasma sus-
taining gas stream suggested a spectroscopic source superior
to those presently in common use. Several investigators were
thus led to explore the analytical capabilities of these
plasmas.

The first investigations documenting the analytical
potentialities of induction-coupled plasmas were performed
by Greenfield et al. (9) in England and independently and
concurrently in this country by Wendt and Fassel (6). Both
groups described their equipment, the characteristics and
appearance of the plasma, and tabulated observed emission
detection limits for several elements in solution. Subse-
quent communications by Hoare and Mostyn (10), Britske
et al. (11), and Veillon and Margoshes (12) have also
reported detection limits observed for trace elements in
solution. Various combinations of plasma operating param-
eters and sample introduction techniques have been employed
by these investigators which are summarized in Table 1.

The 36 MHz plasma employed by Greenfield had a central
axis visibly cooler than the surrounding plasma volume.
Sample aerosols were injected into this cooler region and

Table 1. Comparison of plasma operation

	1964 Greenfield et al. (9)	1965 Wendt and Fassel (6)	1966 Hoare and Mostyn (10)	1967 Britske et al. (11)	1968 Veillon and Margoshes (12)
Frequency (MHz)	36	3.4	36	40	4.8
Plasma gas flow pattern	vortex	coaxial	vortex	--	coaxial
Coolant gas flow (1/min)	17	22	18	--	30
Plasma support gas flow (1/min)	5	0.5	3	--	1.7
Aerosol injector gas flow (1/min)	--	0.5	0.5	--	
Nebulization of sample solutions	pneumatic	ultrasonic	ultrasonic	pneumatic	pneumatic
Solution feed rate (ml/min)	0.1[a]	0.12	0.2	--	0.28 (dry)

[a]Estimated.

emission detection limits in the 1 to 100 µg/ml range were observed for several elements. The depressant effect of PO_4^{-3} and Al^{+3} on Ca emission common in flames was shown to be absent in the induction-coupled plasma. In later publications, Greenfield et al. (13,14) reported detection limits improved by two to three orders of magnitude over previous results with a plasma of 20% nitrogen and 80% argon. The single piece construction, dual tube, vortex flow torch of Greenfield is illustrated in Figure 2B.

Wendt and Fassel's coaxial flow torch is shown in Figure 2A. Their 3.4 MHz plasma was a uniform "tear drop" shape and observed detection limits were generally an order of magnitude superior to Greenfield's first reported values. The PO_4^{-3} and Al^{+3} depressant effect on Ca emission was also absent in this plasma (8). Several other applications of induction-coupled plasmas to analytical spectroscopy have been investigated by Fassel's research group. The applicability of these plasmas to atomic absorption spectroscopy was first demonstrated by Wendt and Fassel (15) and sensitivities and detection limits were reported for several elements. Fassel and Dickinson (16) employed the plasma in a scheme for the analysis of molten metals which is described in detail in this thesis. Barnett (17) and later with Fassel and Kniseley (18) utilized the plasma in a study of the internal standardization principle in emission spectroscopy.
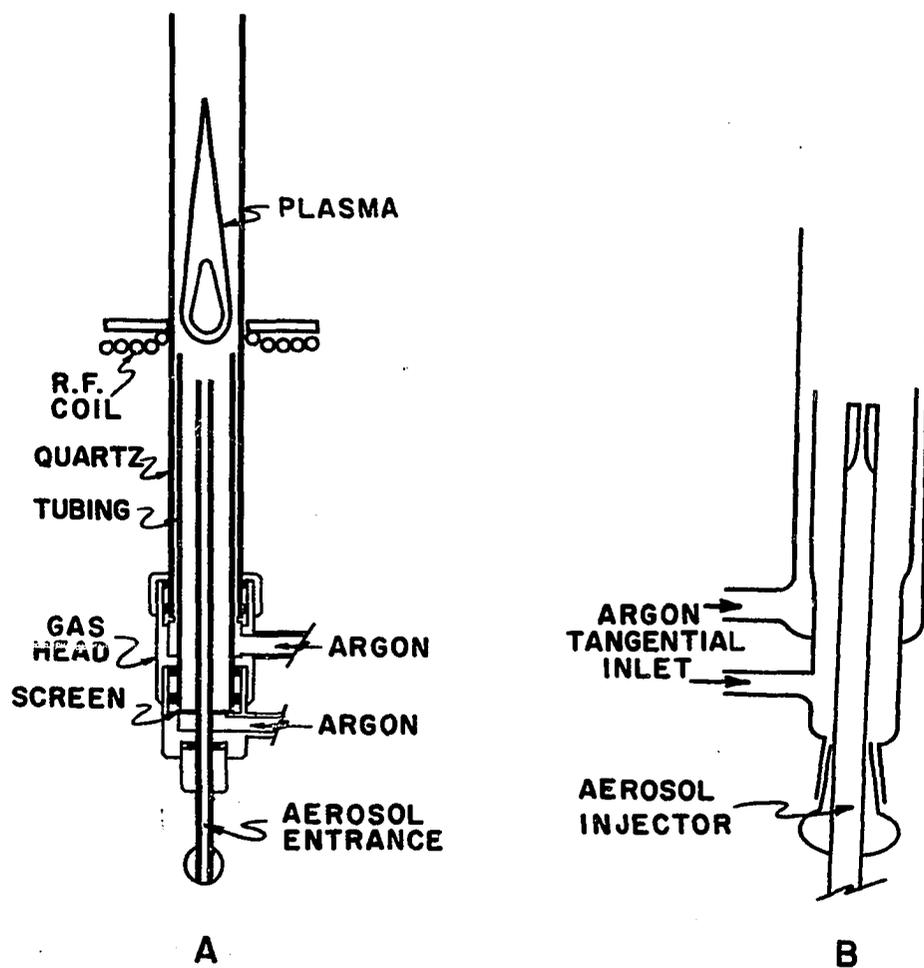
Figure 2. The plasma torch of Wendt and Fassel (6), (A), and Greenfield, et al. (9), (B)

Hoare and Mostyn employed a pure argon plasma and a torch of Greenfield's design for the analysis of B and Zr in Ni alloys. Ultrasonic nebulization of the sample solutions was achieved with a rotating multicell sampling device. Each sample cell was rotated in turn to connect with the aerosol injection gas stream and to locate in the ultrasonic beam. Several detection limits were reported and only a few elements showed a slight improvement over Greenfield's best values. Interference effects on Zr and B emission from high concentrations of various materials present in the sample solutions were shown to be negligible. Hoare and Mostyn also analyzed powdered lithium salts and alumina with the plasma, the first reported application to the analysis of powdered materials.

Details of Britske's operating parameters were very incomplete. The few detection limits presented were approximately equivalent to those observed by Greenfield. An interesting observation was reported however. Under certain conditions, the 40 MHz plasma would transform into a long, thin filament of about 1 mm in diameter. Emission lines originating in high-level energy states were observed from the filament and were described in some detail.

Veillon and Margoshes essentially duplicated the plasma generating facilities and much of the experimental work of Wendt and Fassel. However, pneumatic nebulization with

desolvation of the sample aerosol was employed (19). In contrast to the results of previous investigators, serious interference effects were observed. Instead of a depressant effect on Ca emission from PO_4^- and Al^{+3}, a strong enhancement was obtained. Several other enhancement effects were also observed which the authors were generally unable to explain.

Several of the above communications documented the capabilities of induction-coupled plasmas for the determination of trace elements in solution by tabulation of observed detection limits. Although the values reported were generally superior to those obtained with plasma jet devices (20,21,22), only small improvements in powers of detection over those observed in chemical flames (23,24,25) or microwave excited plasmas (26-29) were realized for a limited number of elements. Emission results from various investigators are tabulated in Table 2 as well as the lowest literature values so far reported for the simple chemical flame excitation source and absorption cell. Before these values can be meaningfully compared, however, the criterion on which they are based must be examined. The detection limits reported by Wendt and Fassel (6) and in the flame emission and atomic absorption references listed in Table 2, were defined as the concentration of the element in solution which gave a line signal twice the statistical fluctuations in the background intensity. In order to obtain an accurate measurement, these fluctuations

Table 2. Comparison of powers of Detection

Element	Detection Limits (μg/ml)					
	1964 Greenfield, et al. (13)	1965 Wendt and Fassel (6)	1967 Britske, et al. (11)	1967 Hoare and Mostyn (10)	1969 Best Flame Emission (23,24,25)	1969 Best Flame Atomic Absorption (30, pp. 60-61)
Al	0.5	3	0.5	0.02	0.01	0.1
Ba	10	-	-	0.002	0.001	0.02
Ca	0.005	0.2	-	0.002	0.0001	0.002
Co	0.2	-	0.1	0.1	0.05	0.005
Cr	-	0.3	-	0.03	0.005	0.005
Fe	0.05	3	-	0.03	0.05	0.005
Mn	0.05	1	0.01	0.05	0.005	0.003
Ni	-	1	0	0.05	0.03	0.005
Pb	0.8	-	0.1	0.3	0.2	0.01
Sn	4	50	-	1	0.3	0.06
Sr	1	0.09	-	0.002	0.0001	0.003
Ta	-	16	-	-	18	6
V	0.1	-	-	0.5	0.01	0.04
Zn	4	-	0.1	1	50	0.02

12

should be of the order 5% of full scale deflection on the recording instrument employed (23). The detection limit concentration would then correspond to a line signal of approximately 10% of full scale deflection. Greenfield's detection limits were defined as that concentration which gave a line signal of only 1% of full scale deflection. Consequently, his detection limits would probably be an order of magnitude higher if they had been based on the fluctuations in background intensity. Hoare and Mostyn defined detection limit as that concentration which gave a line signal just measurable above the background intensity. Had they based their detection limit on the background fluctuations, the values shown in Table 2 would probably be larger by a factor of only two or three. A definition of detection limit was not reported by Britski. Keeping in mind the differences in detection limit definitions. Comparison of the values in Table 2 demonstrates that initial expectations of a superior spectroscopic source in the induction-coupled plasma were not realized.

These disappointing results raised the basic question of whether further refinements in techniques for forming the plasma, for transferring energy into the plasma, and for introducing sample into the plasma would not lead to

realization of the early expectations. The investigation of this question and the application of the induction-coupled plasma to analytical spectroscopy is the subject of this dissertation.

A PLASMA AS AN OBJECT TO BE INDUCTIVELY HEATED

In order to identify the relevant phenomena involved in generating and maintaining induction-coupled plasmas, it is profitable to review certain fundamental principles of induction heating so that these plasmas may be utilized with maximum convenience and efficiency. Details of the principles for the induction heating of various solid materials can be found in several texts such as references 31, 32 and 33.

Skin Effect

A major factor in the induction heating of a material is the "skin effect". The importance of skin effect will become apparent in subsequent discussions. The effect is best illustrated by considering a solid cylindrical conductor within the solenoid inductor as being made up of an infinite number of thin concentric tubes. The rapidly changing axial magnetic field from the inductor induces an electro-motive force in each tube which drives a current within that tube. The induced current flow in any arbitrary concentric tube creates a secondary magnetic field within each tube lying closer to the axis of the cylinder. This secondary field is in opposition to the primary field and induces a back emf which opposes the flow of induced current.

The induced current flow in subsequent tubes adds to this secondary field producing a progressive decay of the primary field and an increasing back emf from the surface to the center of the conductor. The resultant retarding effect on the flow of induced current is illustrated in Figure 3, with x and s defined in equations 1 and 2 below. The current density at any point, x, within the cylinder is represented by the equation

$$I_x = I_o e^{-\sqrt{\frac{\pi \mu f}{\rho}} x} \tag{1}$$

where I_o is the induced current at the surface of the conductor, x is the distance from the surface of the conductor, μ is the relative permeability of the conductor times the permeability of a vacuum $-4\pi \times 10^{-7}$ webers/ampere-meter, ρ is the conductor resistivity in ohm-cm, and f is the frequency of the applied field. The depth within a conductor at which the current density is reduced to $1/e$ (~37%) of the surface value is defined as the skin depth, s, and from Equation 1 is seen to be

$$s = \sqrt{\frac{\rho}{\pi \mu f}} . \tag{2}$$

Therefore, as the frequency of the applied field is increased, the induced current density is confined closer to the surface of the conductor.
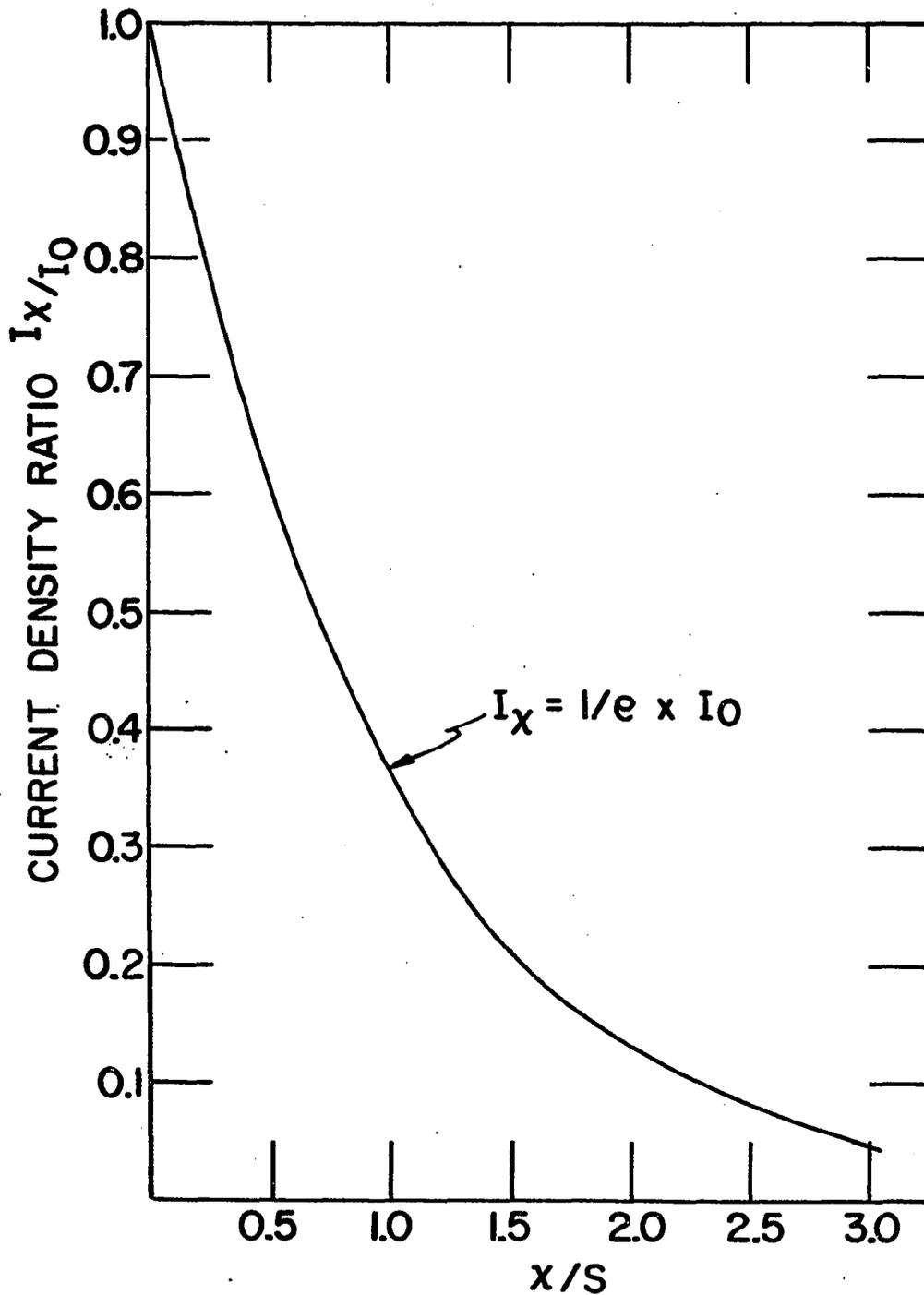
Figure 3. The current density ratio within an inductively heated cylinder versus the ratio of the distance within the cylinder, x, to the skin depth, s, given by Equation 2

Equation 2 however, is only a qualitative approxima-
tion for the skin depth of a plasma, since the plasma does
not behave like a solid conductor. Although the plasma
is a good electrical conductor and its relative permeability
can be assumed equal to unity, evaluation of the plasma
conductivity (reciprocal of resistivity) is difficult
since it changes rapidly across the profile. An average
value must be used, and any estimate is dependent on
temperature which is equally difficult to evaluate.

The conductivity of a plasma is fairly low compared
to solid conductors but increases with increasing temperature,
but not without limit. Rather, a maximum value character-
istic of the plasma gas is obtained. The normal conductivity
ranges for plasmas of three common gases (34) are listed in
Table 3. Hughes and Wooding (35) recently measured the
conductivity of an induction-coupled argon plasma formed with
a 6 kw generator at a frequency of 5.1 MHz and obtained a
value of 30 ± 5 ohm^{-1}cm^{-1}, well within the range of Table 3.
Table 4 shows skin depths calculated with Equation 2 at
various frequencies for the three gases in Table 3. Thus,
at a frequency of 5 MHz, for example, the quartz tube to
contain an argon plasma must be larger than 10 mm in
diameter. As will become evident shortly, the diameter of
the quartz tube should be greater than 4.5 times the
skin depth.

Table 3.   Plasma conductivities of three common gases (34)

Gas	$\sigma(ohm^{-1}cm^{-1})$
Ar	20 - 100
N_2	4 - 20
H_2	1 - 4

Table 4.   Skin depths (mm) for plasmas of three common gases as a function of frequency

Frequency (MHz)	Ar	N_2	H_2
1.0	5 - 10	10 - 25	25 - 50
5.0	2.5 - 5	5 - 10	10 - 25
10.0	1.6 - 4	4 - 8	8 - 20
20.0	1.2 - 2.5	2.5 - 6	6 - 12
30.0	1 - 2	2 - 4	4 - 10

Power and Efficiency

The conditions in a cylindrical conductor may be examined by assuming a uniform magnetic intensity within the solenoid represented by the equation

$$H = I_{(S)} n/l \tag{3}$$

where $I_{(S)}$ is the solenoid current flow in amperes and 1 and n are the solenoid length in cm and the total number of turns respectively. The power absorbed per unit length of conductor within the solenoid is represented by

$$P_{(A)} = \frac{8\pi H^2}{\sigma} \cdot \frac{r}{s} \cdot F. \tag{4}$$

The power is then in watts/cm and F is a Bessel function of the ratio of the cylinder radius to skin depth, r/s. Brown et al. (31, P. 30) have plotted the function F versus the ratio, r/s, for solid cylindrical conductors. This plot is reproduced in Figure 4 and a knee appears in the curve at a value of approximately 2.25 for r/s. For values of r/s greater than 2.25 the function F approaches unity and the absorbed power is near maximum.

The efficiency of energy transfer to the conductor, or efficiency of coupling, is a function of the ratio of the power generated in the conductor to the power lost in the solenoid. The power lost in the solenoid is given by

$$P_{(S)} = I_{(S)}^2 R_{(S)} \tag{5}$$

where $I_{(S)}$ is the solenoid current in amperes and $R_{(S)}$ is the resistance in ohms. The ratio of Equations 4 and 5 is then

$$\frac{P_{(A)}}{P_{(S)}} = \frac{8\pi H^2}{\sigma I_{(S)}^2 R_S} \cdot \frac{r}{s} \cdot F. \tag{6}$$

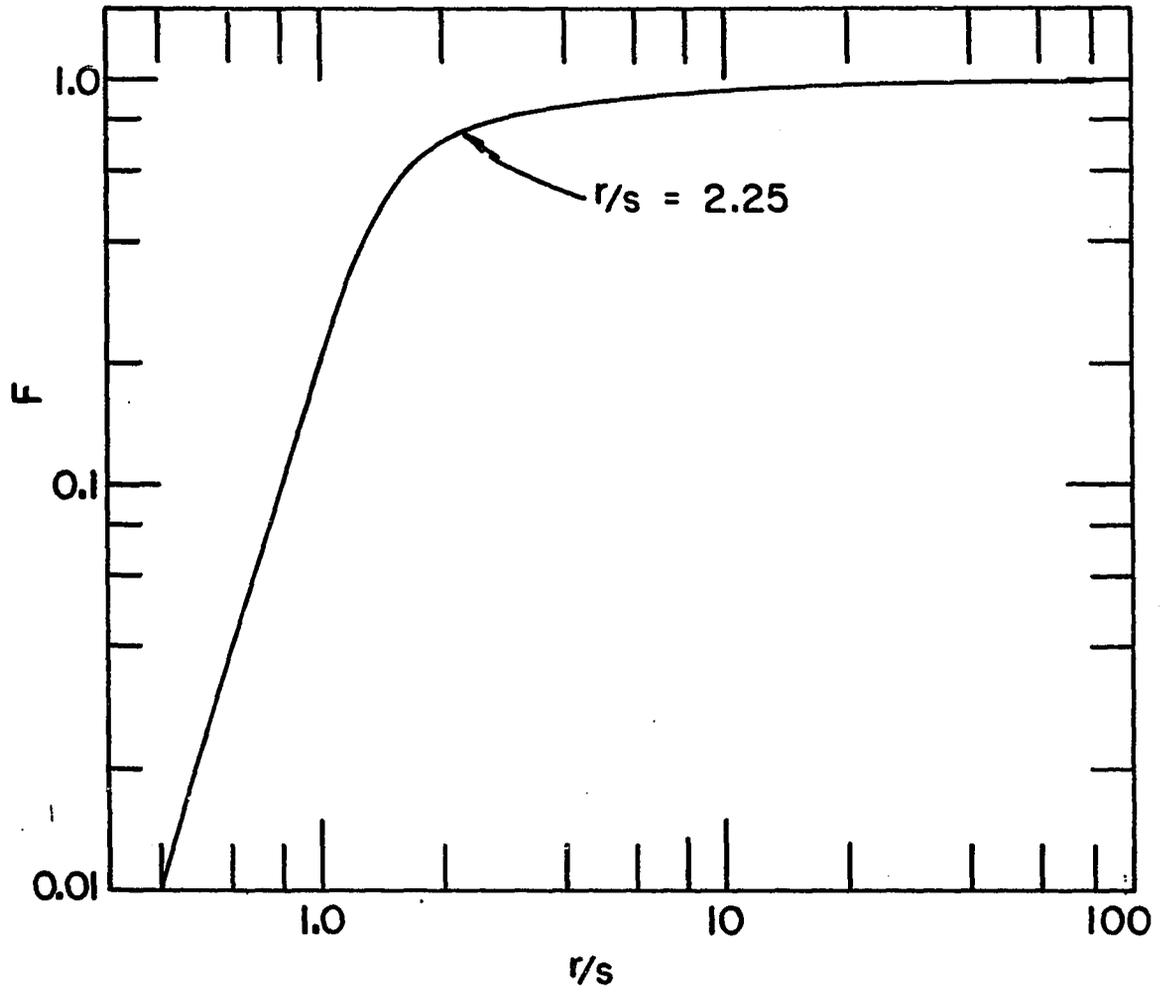Figure 4. The value of the Bessel function, F, versus
the ratio, r/s

Since H is in terms of $I_{(S)}$ and σ and $R_{(S)}$ are in units of ohm^{-1} and ohms respectively, this ratio reduces to only a function of the ratio, r/s, and the plot in Figure 4 is also proportional to the efficiency of coupling. Thus, for a given conductor, maximum power transfer and efficiency of coupling are obtained with a frequency which gives a value greater than 2.25 for r/s.

Mironer and Hushfar (3) applied the above relations to an induction-coupled argon plasma at one atmosphere pressure and found good agreement with energy balance measurements. These observations were also confirmed by Marynowski and Monroe (36), which indicates the plasma behavior is well represented by Equations 2 to 6.

The behavior of Equation 6 at various frequencies was also determined by Mironer and Hushfar (3) and a plot of their results is shown in Figure 5. Examination of this figure indicates the optimum frequency for generating an argon plasma is at and above 10 MHz. This frequency range then apparently corresponds to the region for efficient coupling in Figure 4 where r/s is greater than 2.25. Scholz (1) determined that the optimum coupling efficiency for an argon plasma with a given coil and tube diameter occurred at about 9.5 MHz and was somewhat independent of the gas flow rate. This result is in excellent agreement with the measurements of Mironer and Hushfar.
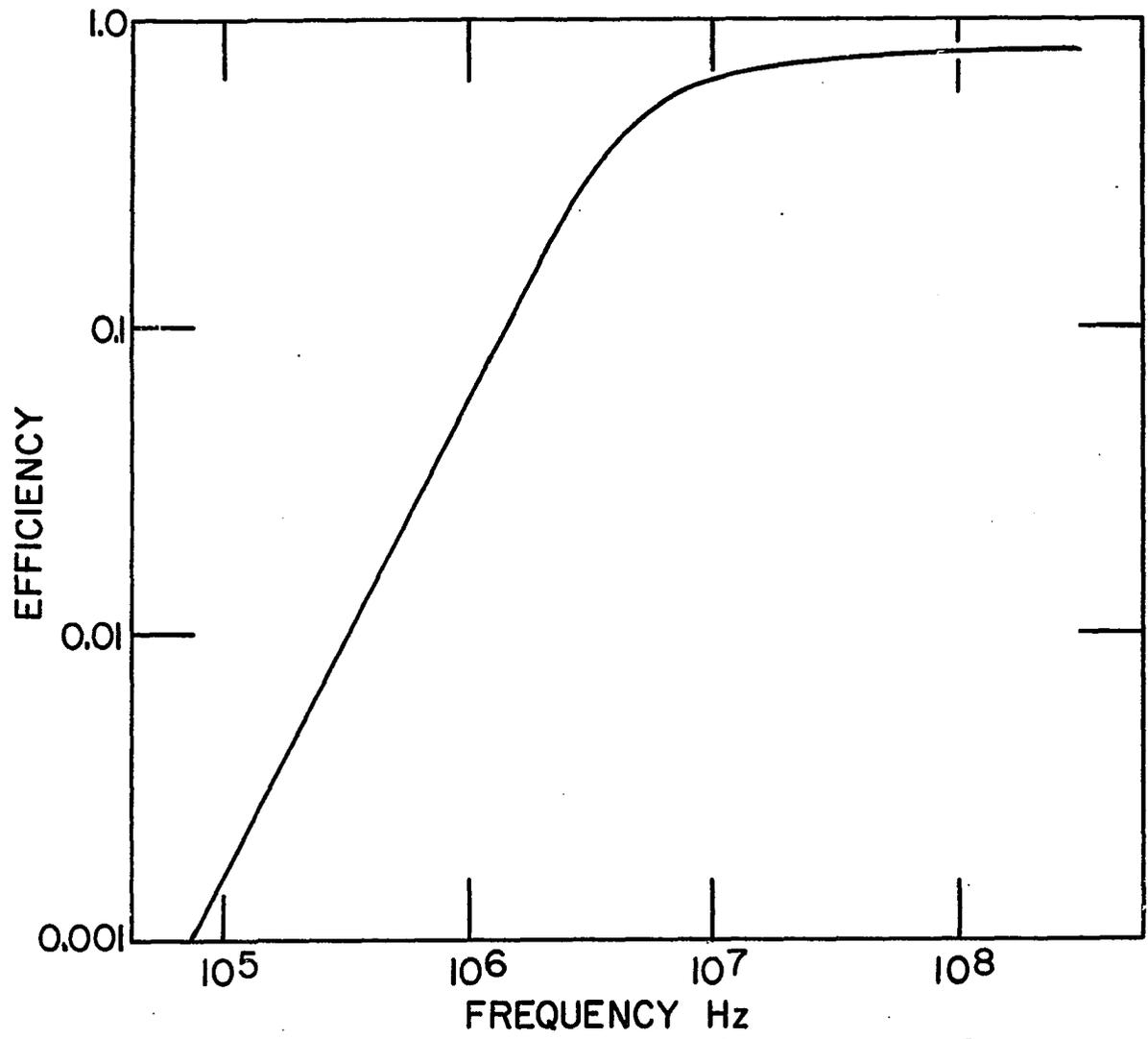
Figure 5.   The efficiency of coupling to an argon plasma versus frequency
of the applied field

The value of 2.25 for r/s indicates that, for efficient coupling of energy, the frequency should be chosen to give a skin depth of less than half the plasma column radius. According to Figure 5, this frequency is 10 MHz or greater for an argon plasma. Two opposing effects are thus apparent in the choice of operating parameters. Increasing the frequency increases the coupling efficiency of the source to the plasma, whereas lowering the frequency results in a more uniform energy distribution within the plasma because of the increased skin depth. At low frequencies the skin depth is large, a large inductor is necessary (from Equation 7) and the source must couple to a large volume of gas. This effect combined with the reduced coupling efficiency at lower frequencies necessitates the application of more power to sustain the plasma.

Of the gases listed in Table 3, argon has the highest conductivity and thus the smallest skin depth for a given frequency. If an argon plasma is generated at optimum conditions, dilution of the argon with a substance of lower conductivity (higher resistivity), such as nitrogen, will decrease the coupling efficiency because of the increased skin depth. Because of the lower conductivity the plasma radius also decreases (37;38,P. 41) reducing the efficiency even further. Two choices are then available to re-establish the maximum efficiency. The power input can be increased

to produce expansion of the plasma and/or the frequency
can be increased to again provide the optimum value of 2.25
for r/s. Diatomic gases, however, also require an appreciable
amount of energy for dissociation leaving less for ioniza-
tion and the need for even more power to sustain the plasma.

During the course of the above discussion, the inter-
action between the performance of the r-f generator and the
plasma has been neglected except for the relationship of
skin depth and efficiency. Another relation which must be
considered is the combination impedance of the plasma-
generator system. The impedance relationship is quite
complex and dramatically influences all of the principles
previously discussed. In order to gain an appreciation for
this complex relationship, a very simplified discussion of
the principles of radio-frequency generation and power
transfer is presented in the following paragraphs.

Radio-Frequency Generation

A simplified circuit diagram of a high frequency
generator is shown in Figure 6. The plate circuit is used
to deliver power to any load and is a parallel resonant
circuit. The basic theory for this circuit is available
in any elementary text on AC circuits and in references
33 and 39. A constant oscillatory current is induced in
the circuit by properly timed current pulses from the
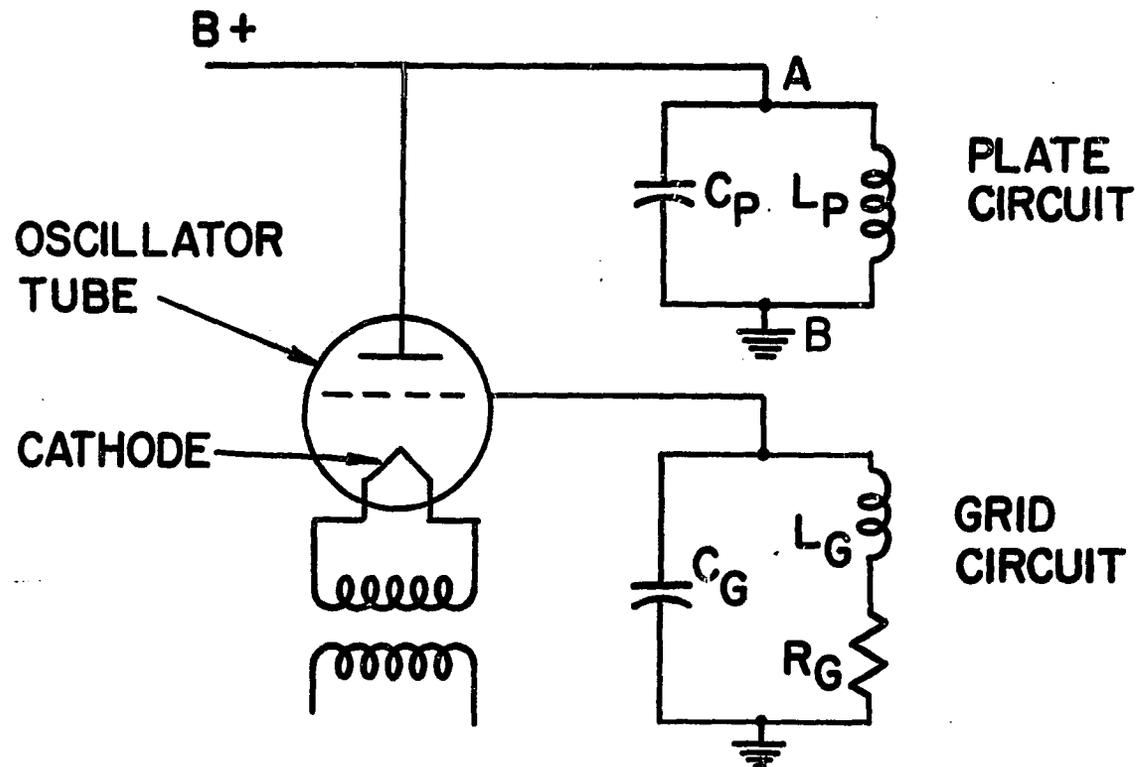
Figure 6.   Simplified circuit diagram of a radio-frequency generator

cathode of the vacuum tube oscillator in the following manner. When the DC voltage is applied to the plate, electrons from the cathode are attracted to the plate producing a current pulse in the plate circuit. The magnitude and duration of this pulse is controlled by the grid of the oscillator tube through a feed back process. A portion of the output energy from the plate circuit is fed back to the grid through either magnetic coupling between the grid and plate inductors or capacitive coupling within the oscillator tube itself. The current pulse in the plate circuit changes the grid potential through the feed back process which stops the flow of electrons from the cathode to the plate. The current stored in the plate circuit capacitor surges back through the circuit restoring the grid potential, again through the feed back process, and the cycle begins again. If this feed back is in phase and of sufficient magnitude, the voltage signals will be additive and will produce self-sustaining oscillations at one frequency, the resonant frequency given by

$$f_{(o)} = \frac{1}{2\pi\sqrt{LC}} \text{ .} \tag{7}$$

The feed back will be in phase when the plate circuit is tuned to a slightly higher frequency than the grid circuit.

Loading the Radio-Frequency Generator

Ohm's law for alternating current is

$$V_{(AC)} = I_{(AC)} Z \tag{8}$$

where Z is the impedance or AC resistance. The power absorbed in an AC circuit is $I_{(AC)}^2 Z$ and for maximum power output, the impedance introduced by the load should be maximized. The loading of a parallel resonant circuit is illustrated schematically in Figure 7. The parallel impedance of the unloaded circuit between A and B is given approximately by

$$Z_{(AB)} = \frac{X_{(L)} X_{(C)}}{Z_{(s)}} \tag{9}$$

where $X_{(L)}$ is the inductive reactance, ωL, ω is the angular frequency, $2\pi f$, L is the inductance in henrys, $X_{(C)}$ is the capacitive reactance, $1/\omega C$, C is the capacitance in farads, $Z_{(s)}$ is the series impedance,

$$\sqrt{R^2 + \left(X_{(L)} - X_{(C)}\right)^2},$$

and R is the series DC resistance around the circuit. At the resonant frequency $X_{(L)} = X_{(C)}$ and the parallel impedance reduces to

$$\frac{L}{CR}. \tag{10}$$

The equation for the effective impedance presented to the

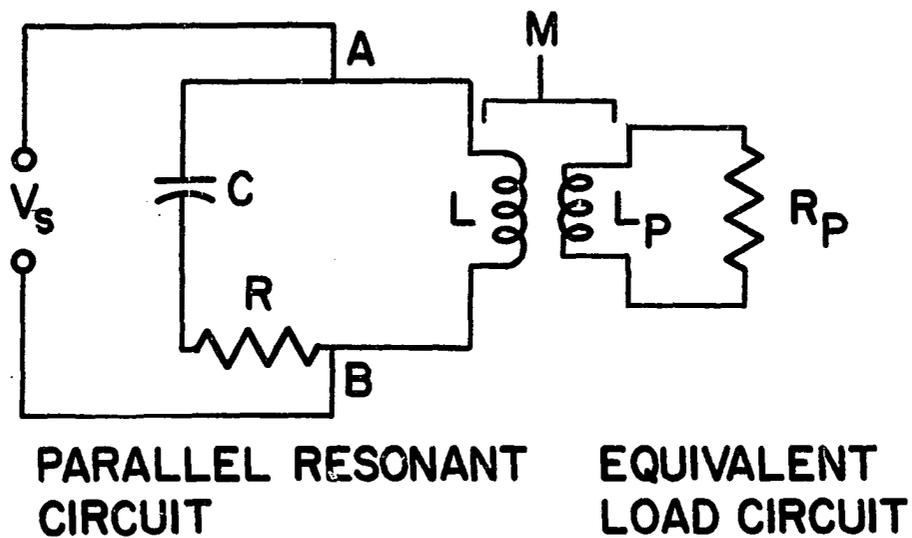PARALLEL RESONANT
CIRCUIT

EQUIVALENT
LOAD CIRCUIT

Figure 7. A simplified circuit diagram illustrating the inductive loading
of a parallel resonant circuit energized by the voltage supply, V_s

voltage supply by the loaded circuit is

$$Z_{(eff)} = Z_{(AB)} + \frac{\omega^2 M^2}{\sqrt{R_{(P)}^2 + X_{(P)}^2}} . \tag{11}$$

M is the mutual inductance between the load inductor and load
equal to

$$k \sqrt{LL_{(P)}}$$

where k is a coupling constant and $X_{(P)}$ and $R_{(P)}$ are the
inductive reactance and resistance of the load. An impedance
is then effectively added in series to the circuit by the
presence of the load.

A general principle of amplifier circuits is that
maximum power output is obtained when the added impedance
due to the load is equal to the unloaded impedance of the
circuit. Referring again to Equation 9, the impedance of
the circuit is maximum at the resonant frequency. A typical
plot of this relation is shown in Figure 8 which reveals the
circuit impedance is drastically reduced by minor deviations
from the resonant frequency. Since the load is coupled to
the circuit through the inductor, the effective inductance
of the circuit is determined by the load which in turn
determines the resonant frequency as given by Equation 7.
Thus, the circuit is designed so that the resonant frequency
is the frequency obtained with a specific load. When the
oscillator is delivering power, the adjustment of proper
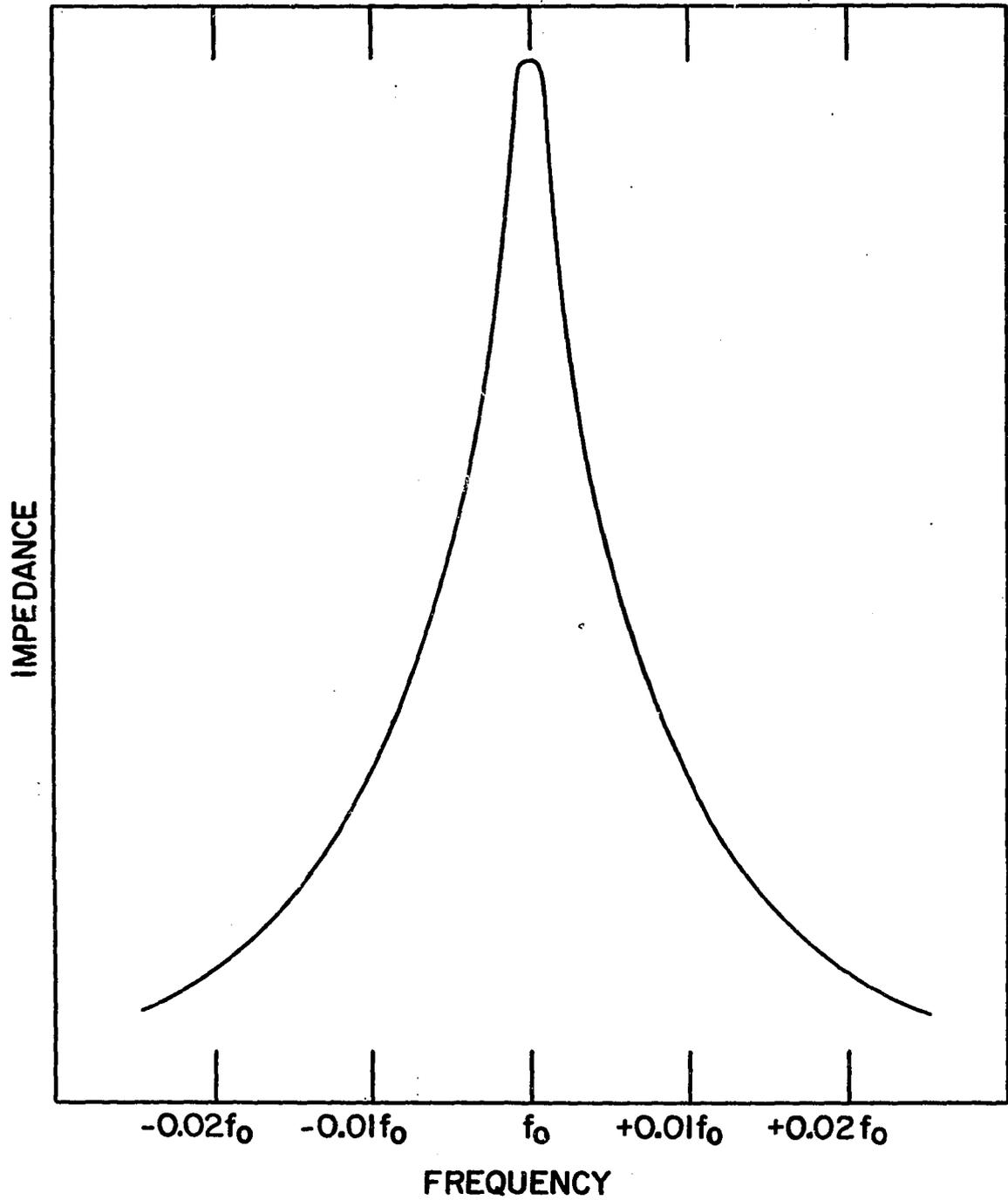
Figure 8. The general impedance behavior of a parallel
          circuit near the resonant frequency

feed back then also depends on loading. If the feed back is not large enough, a small increase in load may throw the circuit out of oscillation. Too much feed back will make the grid current excessively high and power loss in the grid will be larger than necessary. Since power used in the grid is not available as useful output and the oscillator itself supplies the grid power, excessive feed back lowers the overall efficiency. Equation 11 also indicates that for an untuned oscillator circuit such as shown in Figure 6, optimum feed back and maximum power output for a specific coupling arrangement can be obtained for a load of only one specific resistance.

The generation of a plasma with an r-f generator employing a circuit such as shown in Figure 6 presents several problems. The circuit can readily be arranged to provide optimum conditions to sustain a specific plasma, however; initiation of the plasma is difficult. The load resistance without the plasma is nearly infinite, the effective impedance is therefore low, the frequency is off resonance, and considerable reserve power must then be available from the generator to provide sufficient energy to form the initiating pilot plasma. Once the plasma is formed, any variations in the electrical character of the plasma caused by the introduction of foreign material produce deviations from optimum operating conditions. If these

deviations are sufficient, the plasma becomes unstable or
is extinguished.

A more versatile r-f generating system can be provided
if the grid and plate circuits are independently tuned.
Variable capacitors in the grid and plate circuits should
provide such a system. Compensation for minor changes in
feed back, frequency, and effective impedance could then be
achieved by appropriate tuning of the variable capacitors.
In addition, a choice of operating frequencies would be
available.

Magnetically Coupled Circuits

Another approach to providing a versatile r-f generating
system would be the addition of a magnetically coupled circuit
between the load and the generator. A schematic of such an
arrangement is illustrated in Figure 9. The coupling circuit
itself always presents an impedance to the generator governed
by the mutual inductance, M_1. The transformer action of the
combination serves as a "buffer" between the generator and
the load. This action is best illustrated by the general
effect the presence of the coupling circuit has on a typical
impedance, resonance curve as shown in Figure 10. Because of
the flat top of the impedance curve, minor deviations from
the resonant frequency should have little effect on the
power deliverable to a load. A disadvantage of the coupling

GENERATOR
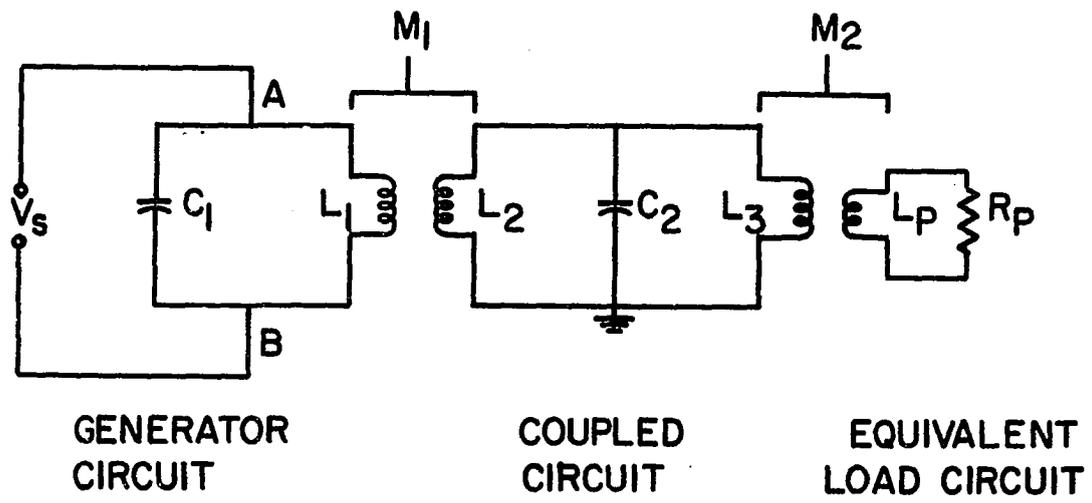CIRCUIT

COUPLED
CIRCUIT

EQUIVALENT
LOAD CIRCUIT

Figure 9.   A simplified circuit diagram of a magnetically coupled parallel
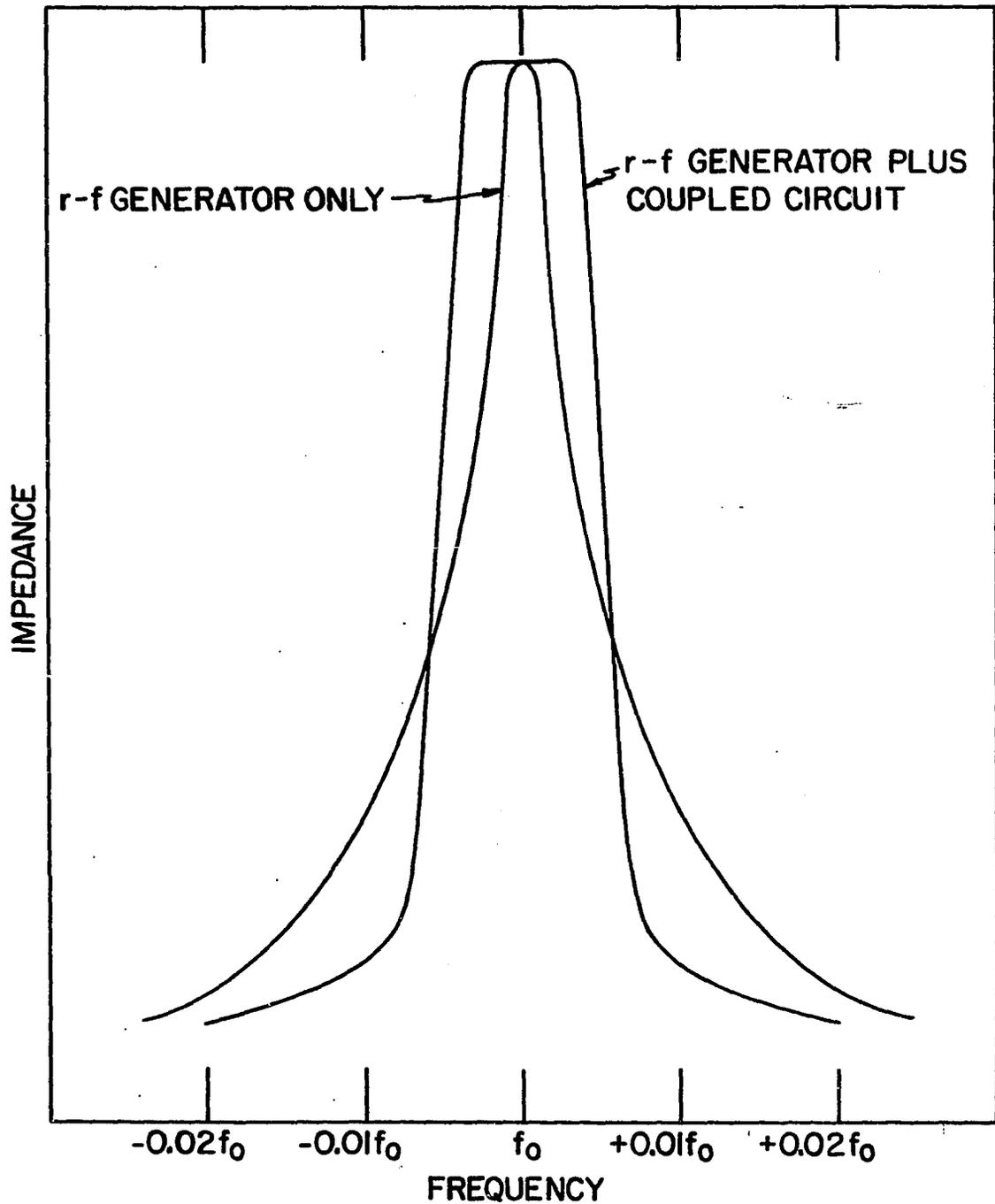resonant circuit between the load and the generator circuit

Figure 10. The general impedance behavior of a parallel circuit magnetically coupled to another parallel resonant circuit

circuit however, is the resistive power loss in the circuit
itself, which would tend to lower the curve in Figure 10
relative to that for the generator only and reduce the power
available to the load.

The effective impedance of the complete circuit including
the load is represented by

$$Z_{eff} = Z_{AB} + k_1^2 \left[\frac{\omega^2 L_1 L_2}{\sqrt{R_{(C)}^2 + \left(X_{(L)eff} - \frac{1}{\omega C_2}\right)^2}} + \frac{\omega_2 M_2^2}{\sqrt{R_P^2 + \omega^2 L_P^2}} \right] \tag{12}$$

where R_C is any resistance contributed by the coupling circuit,
$X_{(L)eff}$ is the effective inductive reactance of the coupled
circuit, and k_1 is the coupling constant previously discussed.
This equation is of the same form as Equation 11 but includes
an interesting difference. The presence of a capacitance
suggests the versatility of the system could be enhanced by
a variable capacitor at C_2. Tuning the capacitor should provide
an additional means of compensating for deviations in the
impedance caused by variations in the electrical character
of the load.

Conclusions

The previous discussion has attempted to briefly outline the basic theory of induction heating and reveal some of the problems involved in developing a compatible plasma-generator combination. Three fundamental and interrelated characteristics are considered to be highly desirable: the generating frequency should be above 10 MHz; the frequency should be maintained as near to the resonant frequency as possible at all times; and, the effective impedance presented to the generator should be maintained constant and as high as permitted for the particular generator employed. The attainment of the above characteristics could only be fulfilled in part with the plasma generating equipment available for this study. The possibilities which were suggested, however, led to the vastly improved plasma generating facility for spectrochemical analysis described in the next section.

PLASMA GENERATING FACILITIES

A versatile induction-coupled plasma generating facility designed for studies in adapting the plasma to analytical spectroscopy should provide: rapid and convenient initiation of the plasma; selectivity and variability of frequency during operation; a means of in operation compensation for plasma impedance variations; and, freedom in selecting specific regions in the plasma for observation. These objectives were substantially realized in practice with the r-f generating equipment chosen for this study.

R-F Generator with Remote Tuning and Coupling Unit

The previous section established the guidelines for development of a versatile plasma-generator combination. Incorporation of variable capacitors in the grid and plate circuits of the generator provided selectivity and variability of frequency during operation. Impedance, coupling efficiency, and feed back could thus be manually controlled. This control, however, was quite critical, so advantage was taken of the "buffering" effect provided by magnetically coupled circuits. Therefore, a remote load coil magnetically coupled to the radio-frequency generator through a variable capacitor was employed. With the remote tuning unit, initiation of the

plasma was remarkably straightforward. Merely tuning the variable capacitor while a carbon rod was in the discharge region resulted in instant formation of the plasma.

The optimum frequency for efficient generation of an argon plasma is 10 MHz or greater as discussed previously. Table 2 of the Introduction revealed the detectability of elements introduced into an argon plasma as observed by Greenfield, et al. (13, 14) and Hoare and Mostyn (10) was superior than that observed by Wendt and Fassel (6). The former investigators employed a plasma generated at a frequency of 36 MHz, whereas the latter employed a frequency of 3.4 MHz. The implication is that frequencies above 10 MHz are also more desirable for the detection of trace impurities in sample materials. For this and other reasons which will become apparent in subsequent discussions, a generator of 2.5 kw output with a variable frequency range of 23 to 50 MHz was chosen for this investigation. A simplified circuit diagram of the generator and remote tuning unit is illustrated in Figure 11. By simultaneous tuning of the grid and plate capacitors, the frequency could be varied during operation over a range of approximately 10 MHz with any one generator coupling coil arrangement. The physical impracticability of simultaneous control of sample introduction and three variable capacitors, however,

PLATE   TUNING UNIT

B$^+$

COUPLING
COILS

LOAD
COIL
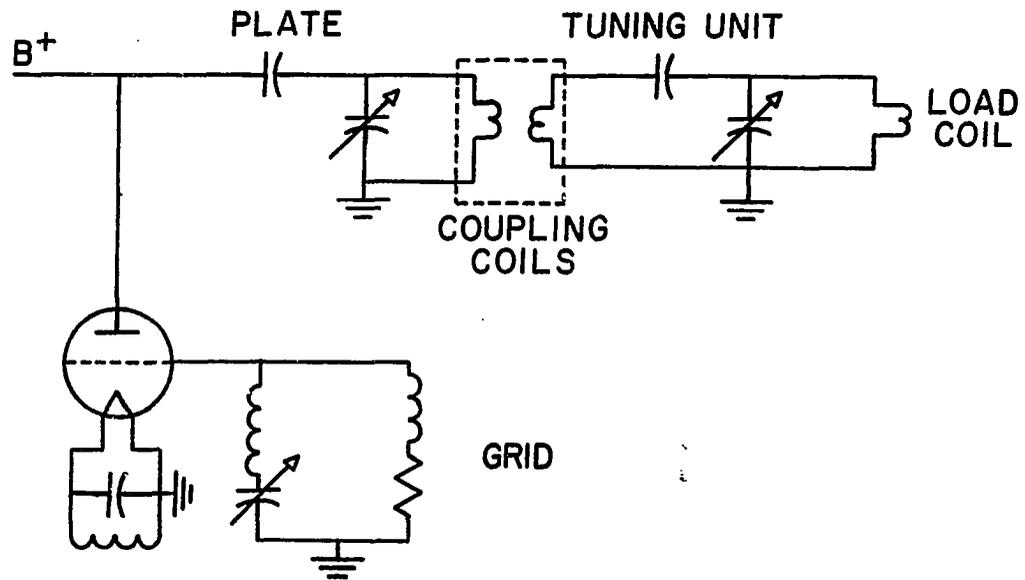
GRID

TUNED-PLATE TUNED-GRID OSCILLATOR 23-50MH$_z$

Figure 11. Simplified circuit diagram of the radio frequency generator
and magnetically coupled tuning circuit

limited impedance control to the remote tuning unit at selected fixed frequencies of the generator.

Because of its relative ease of ionization and inertness, argon was chosen as the plasma support gas. The torch assembly employed was a dual tube, coaxial flow design as described by Wendt and Fassel (6).

Plasma Observation Facilities

Freedom in selecting the point of observation in the plasma was also afforded by the remote tuning unit. The coupling coil was connected to the variable capacitor and load coil through a length of coaxial cable. The tuning unit, plasma torch assembly, and sample introduction facilities were then all mounted on a specially built, movable platform which allowed accurate positioning of any point within the plasma on the optical axis of the spectrometer. A photograph of the complete facility is shown in Figure 12. A facility for the introduction of powdered samples into the plasma is visible in the center of the photograph.

The principle components of the plasma generating facility, plasma torch assembly, and the spectrometer and detector for observing the emitted spectra from the plasma are outlined in Table 5.
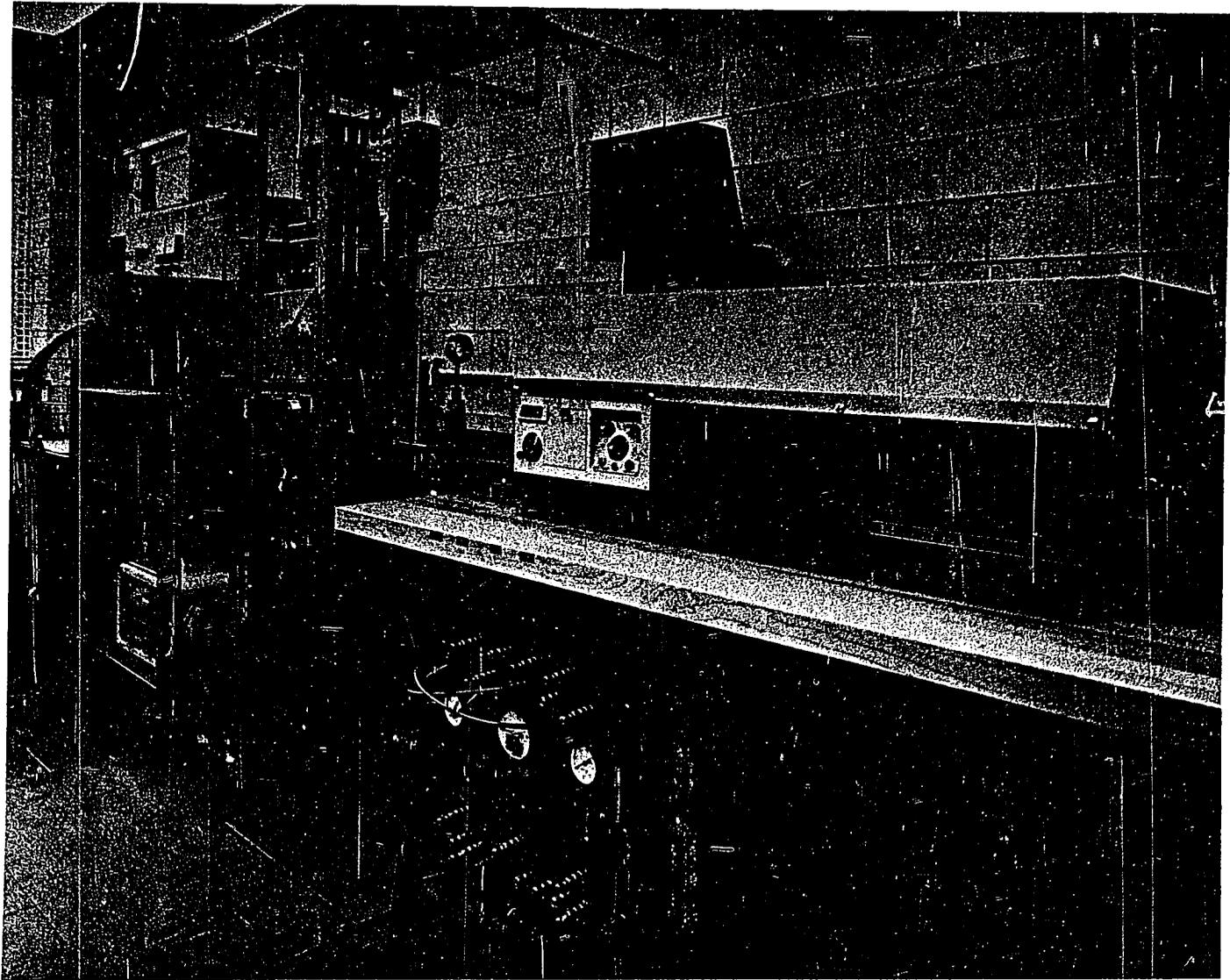
Figure 12. Plasma generation and observation facilities

Table 5. Plasma generation and observation facilities and
          conditions of operation

Apparatus	Description
Plasma power supply	Lepel High Frequencies Laboratory Model T-2.5-1-MC2-J-B generator, frequency variable from 23-48 MHz with attached tuning and coupling unit, 2.5 kw nominal output. The frequency was set at 30 MHz. The load coil was two turns of 5 mm o.d. copper tubing, 24 mm i.d.
Plasma tube assembly	Coolant tube of 18 mm i.d. clear fused quartz 12.5 cm long extending 5 mm above the load coil. Plasma tube of 13 mm i.d. clear fused quartz 13 cm long terminating 2 cm below top of load coil and centered within the coolant tube. The base was of brass construction with double o-ring seals on each tube.
Gas flows	Argon was used throughout with 17 1/min through the coolant tube and 0.75 1/min through plasma tube.
Ignition	Graphite rod, not grounded; lowered into high field region until plasma is formed, then withdrawn.
Spectrometer	Hilger-Engis Model 1000, 1-meter Czerny-Turner mounting scanning spectrometer with 1200 rulings/mm grating blazed for 5000 Å. Reciprocal linear dispersion of 8 Å/mm in the first order.
Slits and order	Both entrance and exit slits were 20 μ wide, 4 mm long, and straight edged. First order spectra were employed throughout.
Detector electronics	The photocurrent from an EMI 6255B phototube was amplified with a Keithley Model 410 picoammeter and recorded with a Leeds and Northrup Speedomax recorder. Time constant was ~3 sec.

DETECTION AND DETERMINATION OF TRACE ELEMENTS IN SOLUTION

The induction-coupled plasma provides a high temperature, contamination free and controllable environment which should constitute an excellent excitation source for spectrochemical analysis. As stated in the Introduction, several earlier communications documented the capabilities of these plasmas for the determination of trace elements in solution by tabulation of observed detection limits. Although the values reported were generally superior to those obtained with plasma jet devices (20, 21, 22), only a very limited list of elements showed small improvements in powers of detection over those observed in chemical flames (23, 24, 25) or microwave excited plasmas (26-29). Reference to Table 2 shows that most of the elements are detectable at lower concentrations in combustion flames than in induction-coupled plasmas. The failure to realize results even comparable to combustion flames with the plasmas employed thus far suggested one or more serious deficiencies in the adaptation of these devices to analytical problems. Initial studies were therefore directed towards an identification of the deficient factors. These studies demonstrated that vast improvements in powers of detection may be achieved through effective utilization of plasma

properties, and in techniques for introducing nebulized sample into the plasma. With the facility employed in this investigation, the detection limits for many elements were reduced to concentrations four to five orders of magnitude lower than those so far obtained by flame atomic absorption or emission spectroscopy.

Sample Introduction into the Plasma

Several investigators have called attention to the difficulties encountered in introducing aerosols or powdered samples into high temperature plasmas (40, 41). These difficulties are readily apparent with induction-coupled plasmas as well. In concurrent studies on the introduction of powdered samples into the plasma, the solid particles were observed to simply reflect from or to pass along the outer surface of the plasma, as shown in Figure 13. The skin depth effect of induction heating was turned to good advantage in improving this situation. In an established induction-coupled plasma, the eddy current flows in a more confined path closer to the outer circumference of the plasma as the frequency is increased. In this way a toroidal shaped plasma (see Figure 13) may be formed. The cooler "doughnut hole" entry provided by this configuration presents far less resistance to the injection of aerosol particles into inner regions of the plasma. Injected sample particles therefore pass through an axial channel in the

LOW
FREQUENCY

HIGH
FREQUENCY

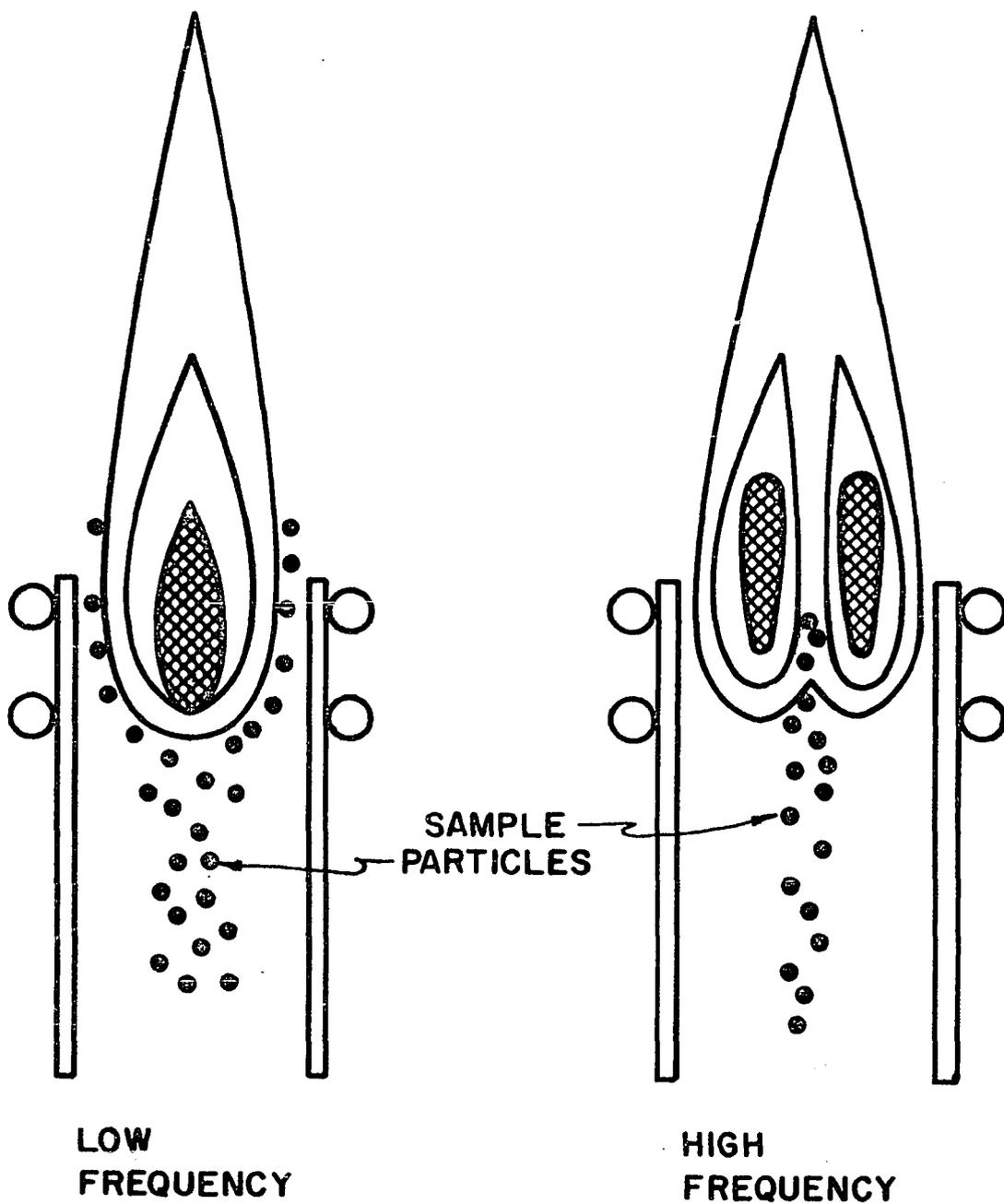SAMPLE
PARTICLES

Figure 13.   Aerosol entry into uniform versus toroidal
             shaped plasma

center of the plasma where they are heated by radiation and conduction. The particles are also confined to a finite emitting volume rather than being spread over the entire surface of the plasma. Both the generating frequency and the flow velocity of the argon stream which injects the entrained aerosol into the plasma affect the degree to which the toroidal shape is developed. As a consequence, con-- siderable control may be exercised on the thermal environment experienced by the sample aerosol during its transit through the plasma. The vastly improved powers of detection reported later in this thesis were obtained at a generating frequency of 30 MHz and an argon flow of 1.7 1/min through the injection orifice.

Ultrasonic Nebulization

The use of ultrasonic energy for the formation of aqueous aerosols has recently received attention from practicing spectroscopists (6, 10, 42-50). The attraction for ultrasonic nebulization stems from three distinct advantages over conventional pneumatic nebulization techniques: the formation of the aerosol is independent of the gas flow rate; the diameter of the particles formed is of the order of a few microns; and, the aerosol can be transported with a relatively low velocity gas flow. Thus, the delivery of aerosol to any specific spectroscopic source can be accurately controlled.

Basic theory

When the ultrasonic energy encounters the surface of a liquid, capillary waves are produced. According to Kelvin (51), the wavelength of these waves is

$$\lambda = \left[\frac{8\pi\sigma}{\rho f^2}\right]^{1/3} \tag{12}$$

where λ is the wavelength, σ the surface tension, ρ the liquid density, and f the ultrasonic frequency. If sufficient ultrasonic energy is applied, the capillary waves are ruptured at the liquid surface to produce droplets. The size of the droplets has been experimentally determined by Lang (52) to be

$$D = 0.34 \; \lambda \tag{13}$$

where D is the median droplet diameter, and λ the capillary wavelength according to Equation 12. Peskin and Raco (53) theoretically derived an equation for the size of ultra-sonically produced droplets and confirmed the results of Lang. The calculated median droplet diameter for the 800 KHz generator employed in this study is $\sim$ five microns. The gas flow necessary to transport the aerosol droplets must be in excess of the droplet terminal velocity, which can be readily calculated using Stokes' law.

Desolvation of the Sample Aerosol

Aerosol feed rates in the range of 0.05 to 0.2 ml/min have been employed by previous investigators. Although not explicitly stated in the earlier publications (6, 9, 10, 13, 14, 15) the amount of solvent which may be introduced into the plasma is limited by the poisoning action of the molecular gases released. These molecular gases not only cause an impedance mismatch but also absorb energy from the plasma for their excitation and dissociation. The energy available for the plasma-sustaining ionization of the argon support gas is therefore diminished. Unless additional power from the radiofrequency generator is supplied, the plasma becomes unstable and extinguishes as the molecular gas concentration is increased. Appropriate tuning of the variable capacitor of the remote tuning unit permitted the introduction of aqueous sample aerosol into the plasma at a rate of approximately 0.3 ml/min. This rate was three times the rate permissible with a previous plasma generating system employed in this laboratory, however; an even higher sample introduction rate would be desirable in obtaining maximum element detectability.

Another approach to overcoming this limitation is desolvation of the sample aerosol. This technique has been found beneficial in improving powers of detection in flame atomic emission (54) and atomic absorption (55, 56) but for other reasons. During the course of this investigation,

Veillon and Margoshes (19) described a desolvation facility specifically adapted to plasma emission studies. The facility illustrated in Figure 14 and described in detail below is similar in principle to the Veillon-Margoshes apparatus, except that ultrasonic rather than pneumatic nebulization is employed. With the desolvation facility in operation, the nebulization rates could be increased to 0.63 ml/min, and powers of detection were typically improved by a factor of five.

Ultrasonic Aerosol Generation and Desolvation Apparatus

The general construction of the aerosol generator was patterned after the designs of West and Hume (42) and Wendt and Fassel (6). The complete facility is illustrated in Figure 14 and the pertinent details which apply to the aerosol generator itself are found in Table 6.

To assure long term stability of the nebulization rate, the transducer, the water coupling bath, and sample solution were maintained at nearly constant temperature ($\pm5°C$) by the water cooling system. The sample solution accommodated 100 ml and a constant sample solution level was maintained by continuous addition of sample via an infusion pump at the 0.63 ml/min nebulization rate.
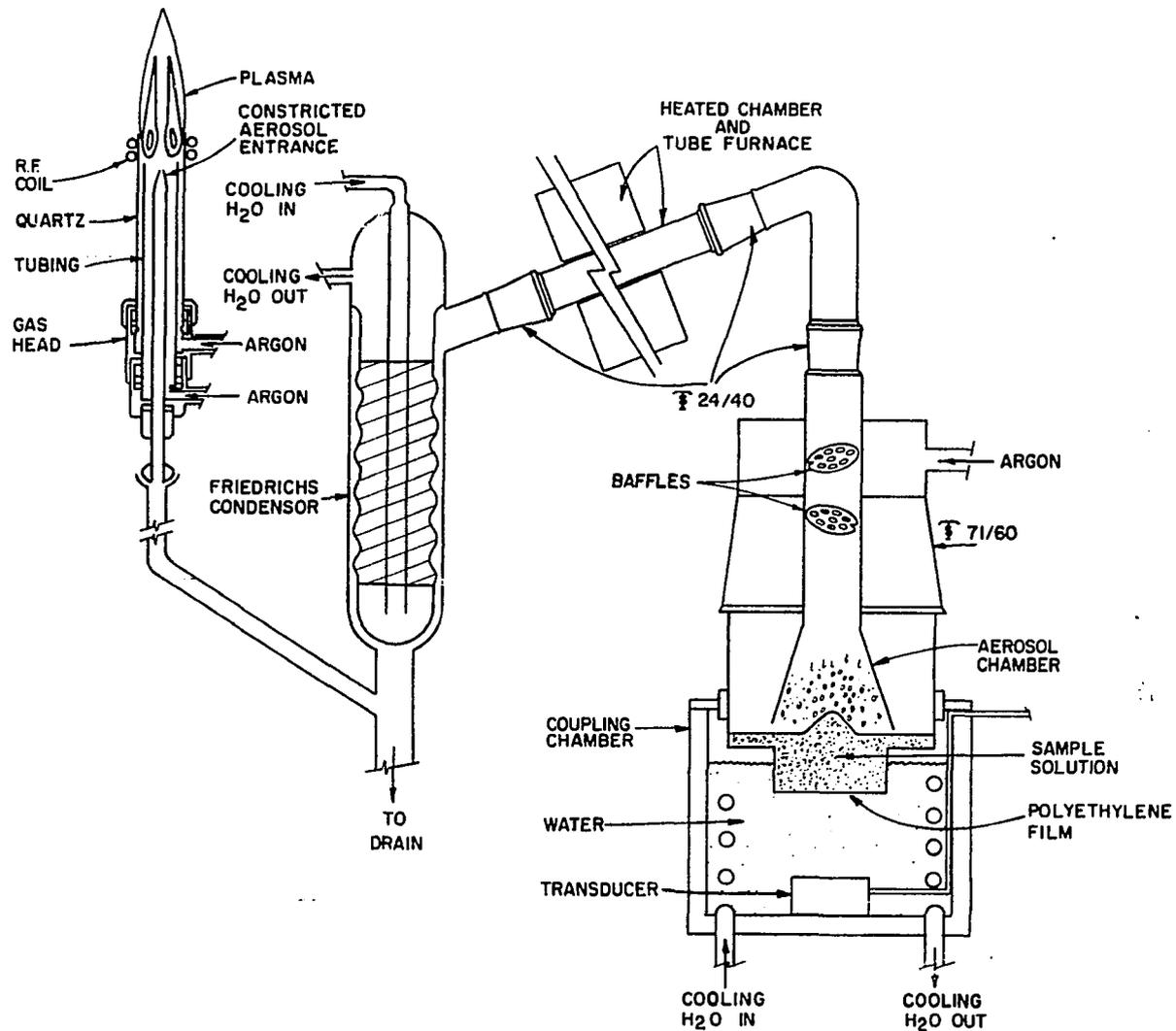
Figure 14. Schematic diagram of ultrasonic aerosol formation, aerosol desolvation, and plasma excitation facility

Table 6. Experimental facilities and operating conditions

Apparatus	Description
Aerosol generator	Macrosonics Corporation Model 250 FF ultrasonic generator, 80 watts nominal output; type A-800 transducer, 2.5 cm i.d., 0.25 cm.thick, 800 KHz frequency, driven at 25% of full power.
Coupling chamber	2 liter beaker with ~12 cm coupling water between transducer face and bottom of sample chamber. Coupling water temperature maintained by tap water cooling.
Sample container	Inner glass joint $\mathfrak{F}$ 71/60 with a bottom of 4.5 cm i.d. covered with 0.03 mm polyethylene, 100 ml capacity.
Aerosol chamber and baffles	Outer glass joint $\mathfrak{F}$ 24/40 18 cm long, flared to 5 cm i.d. at bottom, and sealed into $\mathfrak{F}$ 71/60 outer glass joint with argon inlet. Two perforated polyethylene disk baffles were positioned in aerosol chamber as shown in Figure 14.
Tube furnace and desolvation chamber	A 2.5 cm i.d. quartz tube through 20 cm long, 2.8 cm i.d. tube furnace maintained at ~400°C.
Condenser	Friedrichs condenser with side arm outlet to plasma, tap water cooling.
Aerosol delivery tube and gas flow	A tube of 7 mm dia. borosilicate glass constricted to 1.5 mm i.d. at the tip terminating at the top of the plasma tube. A 1.7 l/min flow of Ar was used to deliver the aerosol to the plasma.
Solutions	Stock solutions were prepared by dissolution of pure metals or reagent grade reagents in dilute acid or distilled water. Samples were distilled water dilutions of the stock solutions.

Table 6. Continued

Apparatus	Description
Average sample nebulization rate	0.63 ml/min
Plasma generating frequency	30 MHz

Performance

The amount of aerosol delivered to the desolvation facility depends, as expected, on the rate at which the aerosol is produced and on the flow of argon which transports the aerosol from the aerosol chamber. In order to simplify terminology, the flow of argon used to transport the sample aerosol is hereafter termed the aerosol gas flow. The rate of aerosol production is, of course, a function of the power output from the ultrasonic generator. As the ultrasonic power was increased, however, emission intensities from elements in sample aerosols introduced into the plasma became less stable. Presumably, this decrease in stability was caused by random pressure pulses induced in the aerosol gas stream. Hell, et al. (56) observed emission instabilities caused by pressure pulses in the gas stream of a commercial pneumatic nebulizer and desolvation apparatus used in flame atomic absorption spectroscopy. In the facility shown in Figure 14, however, the violent turbulence induced in the

sample solution by the ultrasonic energy apparently creates
these pressure pulses which are then manifested in the plasma
as fluctuations in emission intensity. At power settings
above 25% of full power on the ultrasonic generator, the
plasma was observed to periodically "bounce" and emission
intensity measurements of acceptable reproducibility could
not be made. Hence, the power setting on the ultrasonic
generator was maintained at 25% throughout this investigation.
Baffles were also added to the neck of the aerosol chamber
to smooth the flow of aerosol and improve emission stability.
In Figure 15, the sample delivery rate obtained with the
baffles in place and the ultrasonic generator set at 25% of
full power is plotted at various aerosol gas flow rates. The
solution delivery rate was not measured at argon flow rates
above 2 l/min for reasons discussed in the next section.

As expected, a fraction of the dehydrated aerosol was
lost in transit through the desolvation facility. Of the
total solids in the sample solution nebulized, approximately
80% was transported to the plasma. This figure was deter-
mined indirectly from a nebulized 50 μg/ml Fe solution.
Plasma emission analysis of the combined solvent condensate
and washings from the heated chamber and condenser revealed
that 20% of the Fe nebulized was retained in the desolvation
facility. The effectiveness of water removal was demonstrated
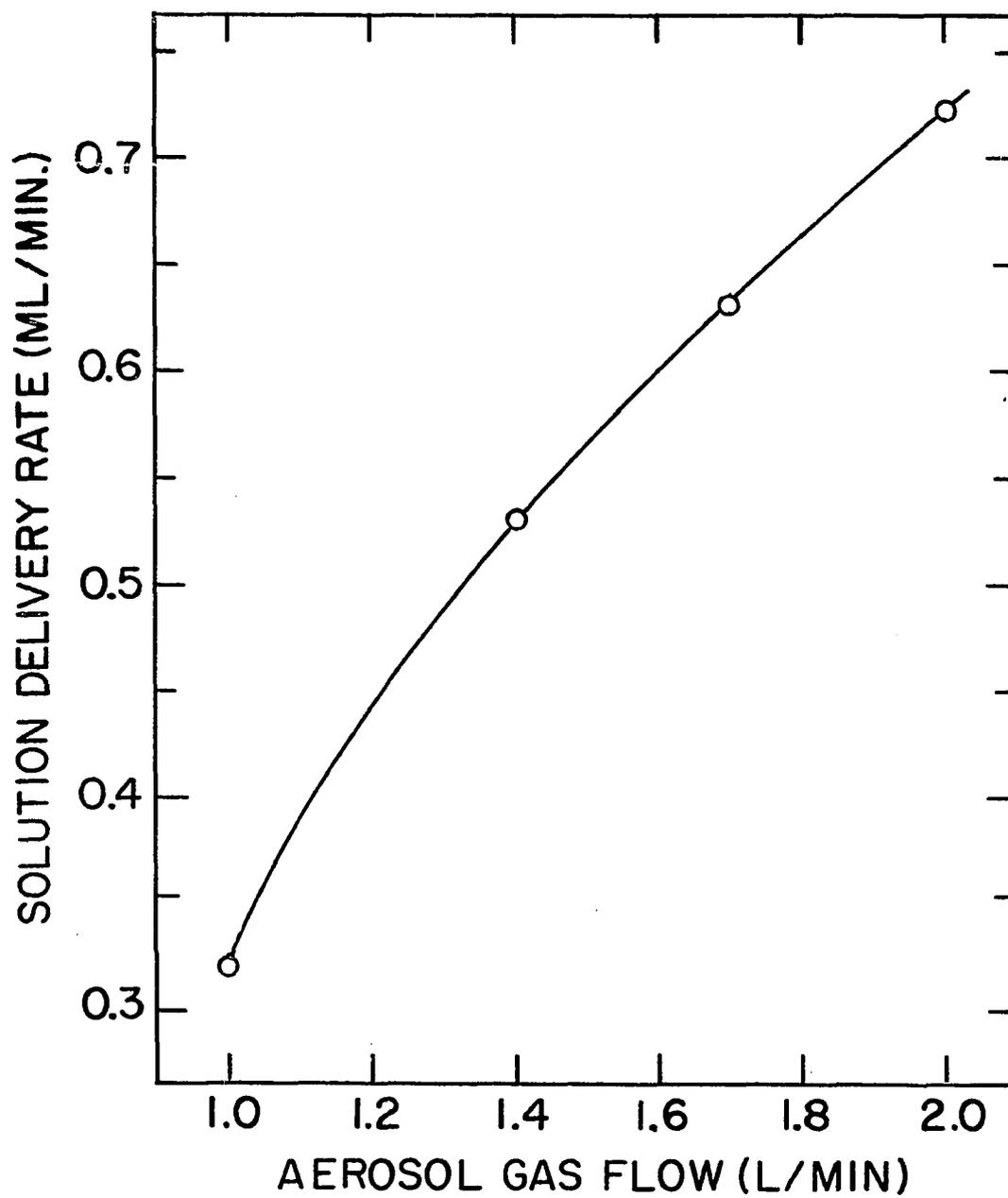by the absence of any increase   in the OH 3064 Å band head

Figure 15. Measured sample solution delivery rate versus aerosol gas flow

intensity over that obtained from impurities in the argon supply.

Sample Behavior in the Plasma

Containment of injected sample particles within the axial channel through the center of the plasma was confirmed by horizontal profiles of the emission intensity from a 50 μg/ml Fe solution. Figure 16 shows the intensity obtained from the Fe I 3719.9 Å line at two vertical positions in the plasma. The zero on the horizontal axis is the center of the plasma.

The emission intensities obtained from elements introduced into the 30 MHz toroidal shaped plasma and a uniform shaped plasma provide an interesting comparison. The emission intensity of the Th II 4019.1 Å line obtained from a 50 μg/ml solution in the toroidal shaped plasma is shown in Figure 17B and a uniform shaped plasma in Figure 17A. The emission intensity is increased by over two orders of magnitude in the toroidal shaped plasma and, in addition, the background intensity is reduced by approximately two orders of magnitude. The same comparison is shown in Figure 18 for a 10 μg/ml Ni solution. The emission intensity of the Ni I 3524.5 Å line in the toroidal shaped plasma (Figure 18B) is over an order of magnitude greater and the background intensity is again approximately two orders of magnitude
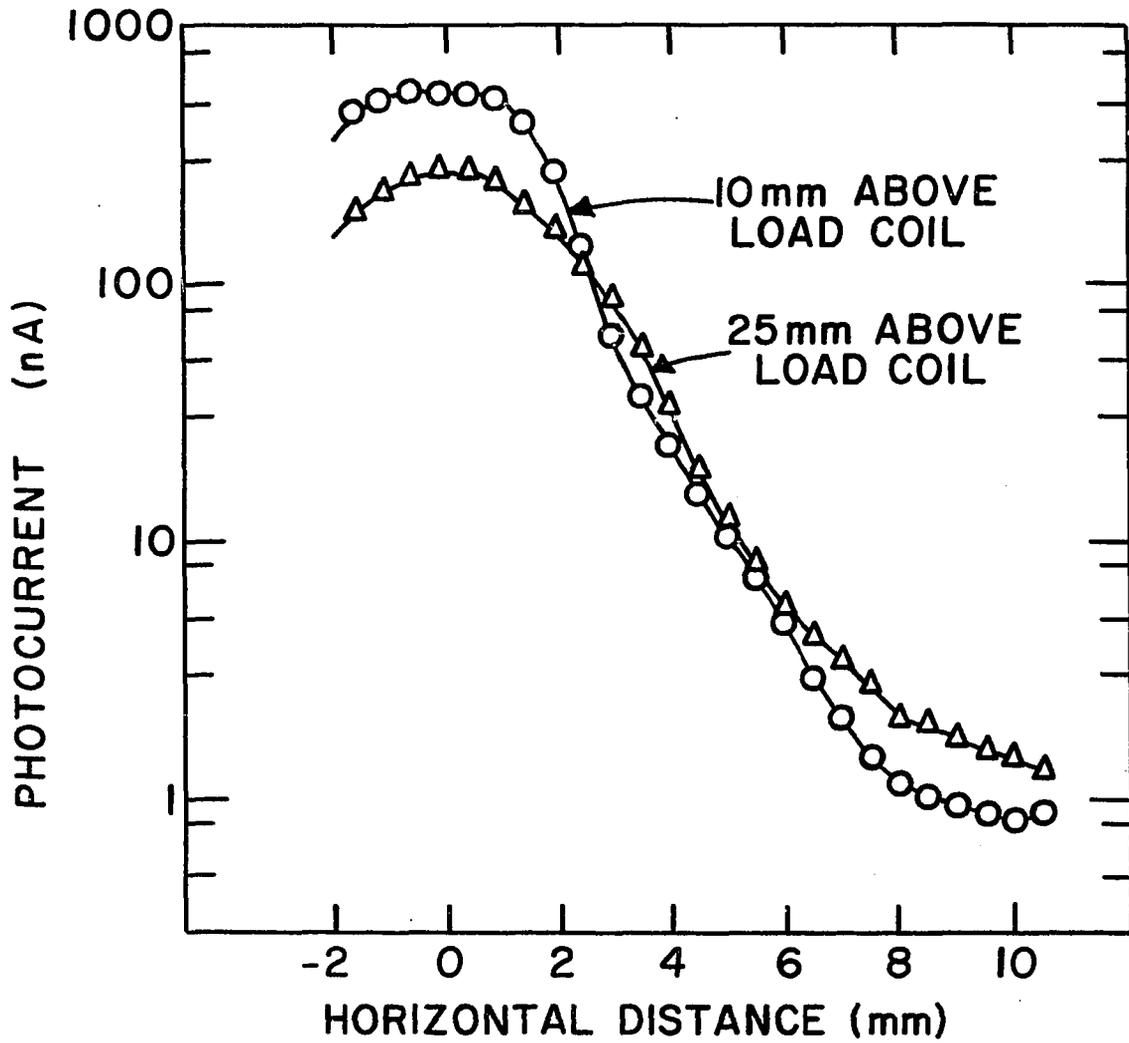
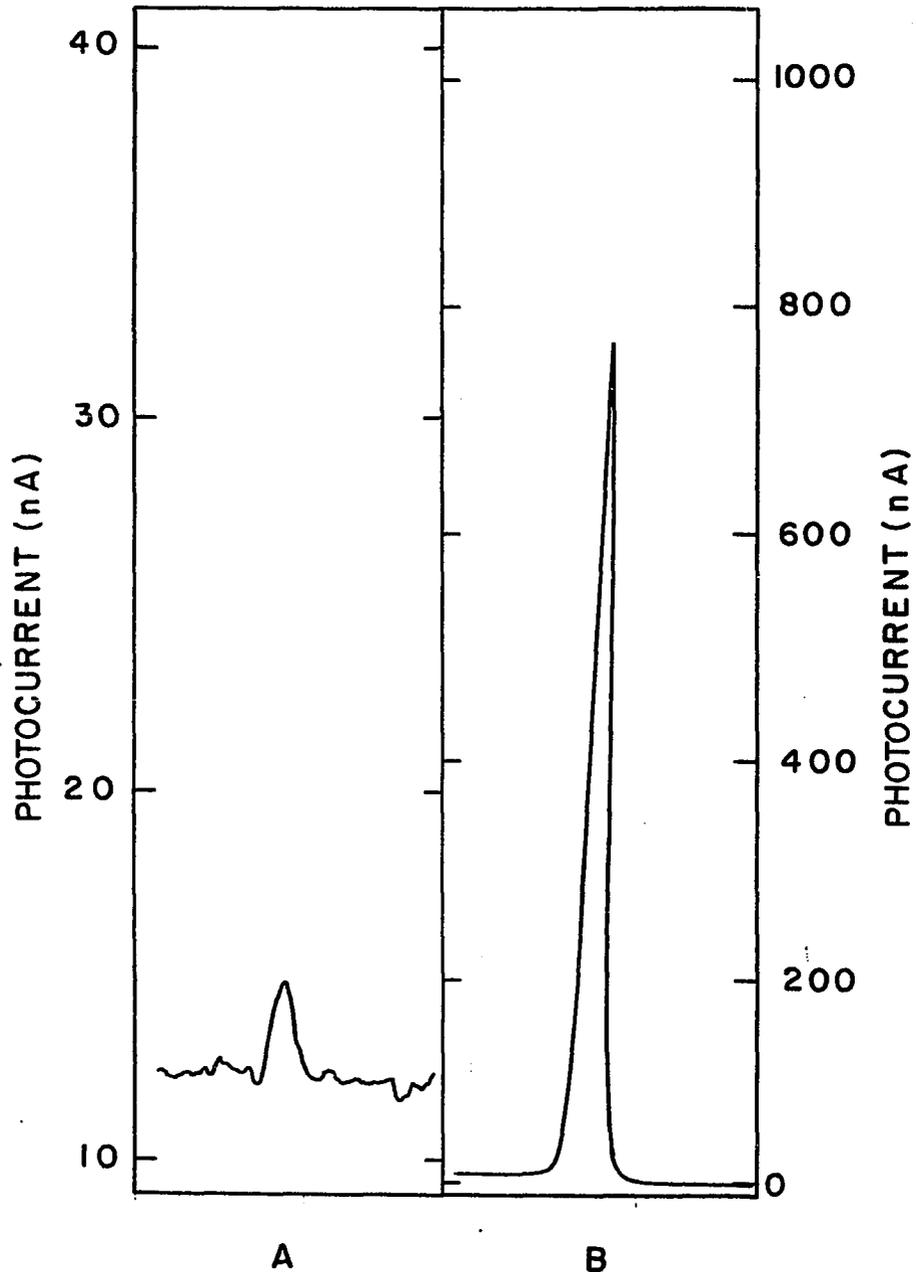Figure 16. Horizontal profile of the emission intensity from 50 μg/ml Fe at two vertical positions above the load coil

Figure 17. Observed emission intensity from 50 μg/ml Th
in a uniform shaped plasma (A) and the 30 MHz
toroidal shaped plasma (B)

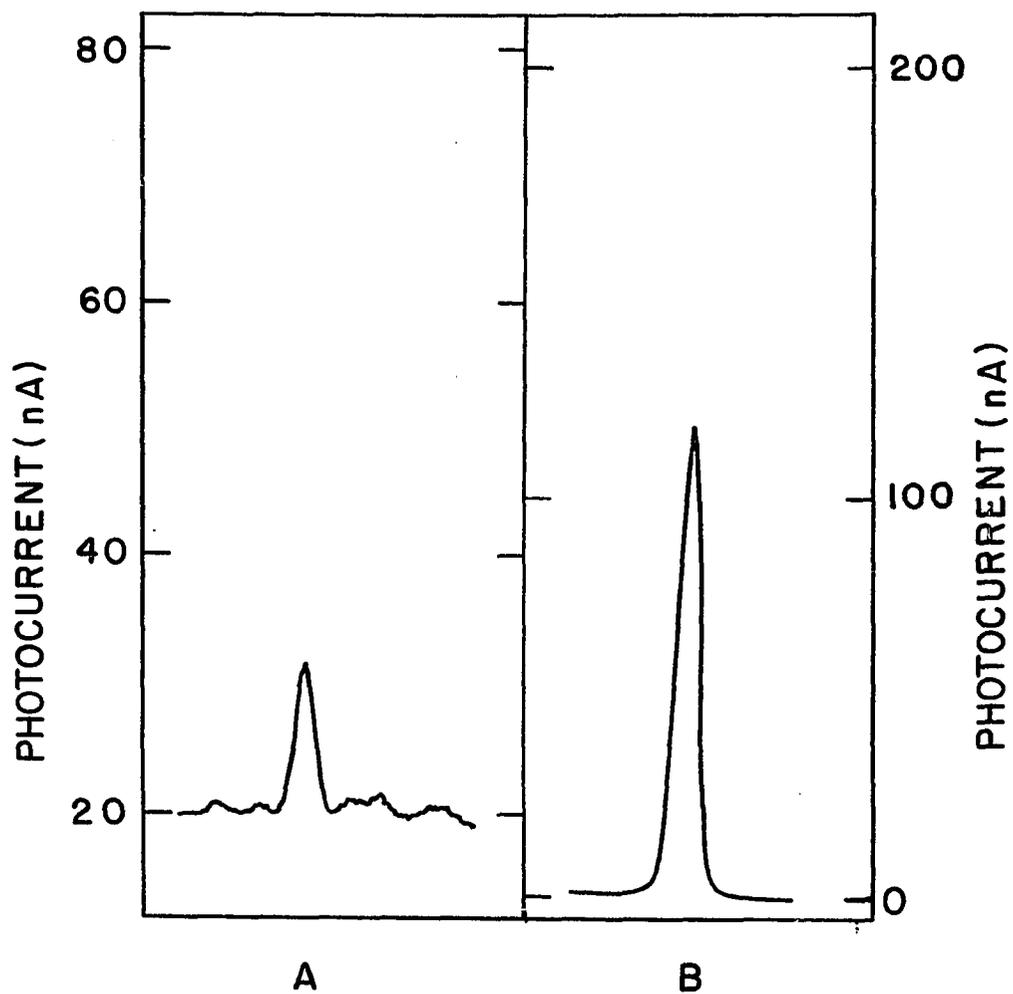Figure 18. Observed emission intensity from 10 μg/ml Ni
in a uniform shaped plasma (A) and the 30 MHz
toroidal shaped plasma (B)

less than in the uniform shaped plasma (Figure 18A). An

approximate calculation indicates an increase in intensity

of only seven- to nine-fold should result from confinement

of the sample in the axial channel of the toroidal shaped

plasma as compared to the sample being spread over the sur-

face of the uniform shaped plasma. Consequently, the degree

of excitation in the toroidal shaped plasma must be considerably

higher than in the uniform shaped plasma.

The emission spectrum between 3,000 and 4,000 $\overset{\circ}{A}$ from a

1 μg/ml Ni solution introduced into the toroidal shaped

plasma is shown in Figure 19. This figure illustrates the

intensity and complexity of the emitted spectra resulting

from typical elements passing through the plasma. The

spectra are considerably more complex than those obtained

from chemical flames and are similar to those emitted from

a dc arc.

Vertical profiles of the axial channel revealed the

position in the plasma and the flow of aerosol gas for

maximum element detectability. Figures 20 and 21 are

typical of the profiles obtained for several elements. Of

the elements profiled, all exhibited maximum detectability at

an aerosol gas flow of either 1.7 or 2.0 1/min. Evidently,

the shorter sample residence time in the plasma at higher

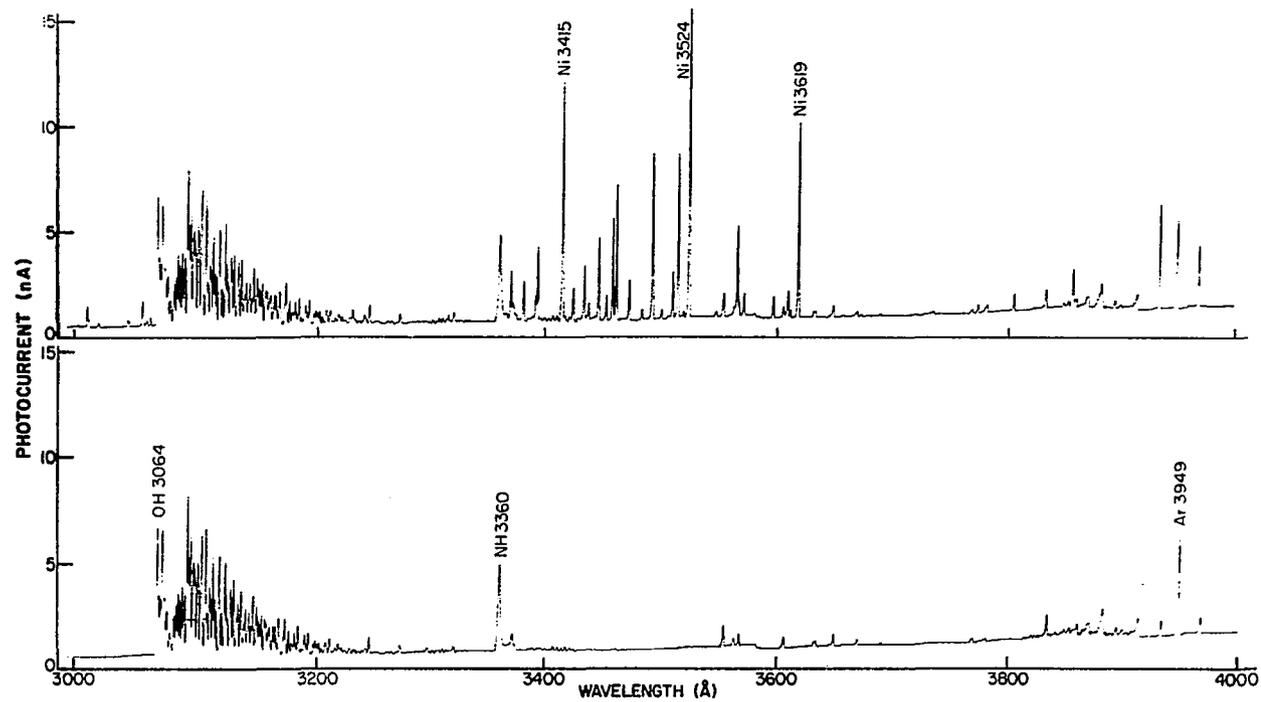flow rates precluded any increase in intensity from the

Figure 19. Emission spectra from the plasma for a 1 μg/ml Ni solution (upper) and pure water (lower)
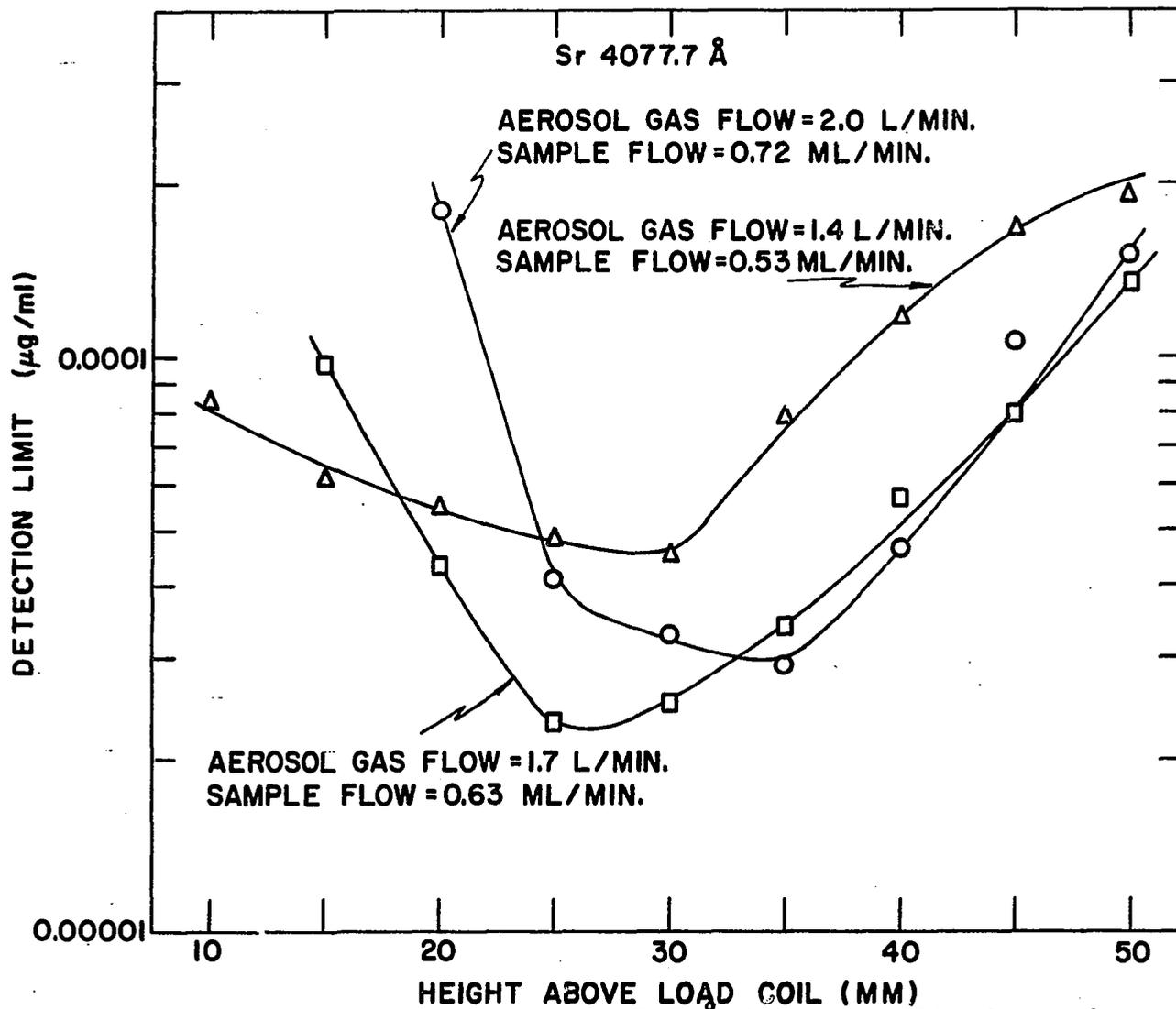
Figure 20. Vertical profile of the Sr 4077.7 Å detection limit at three aerosol gas flow and sample solution delivery rates
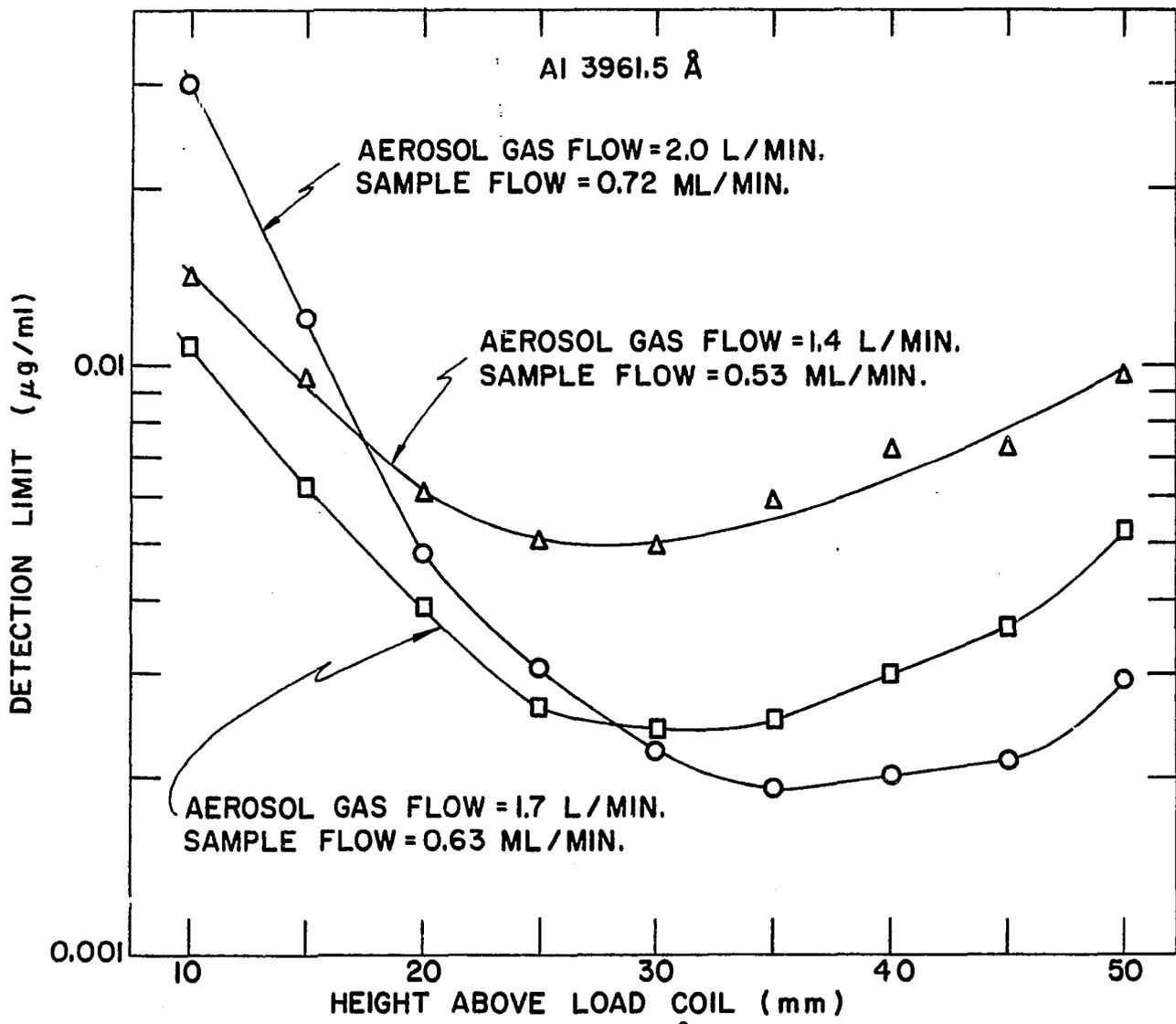
Figure 21. Vertical profile of the Al 3961.5 Å detection limit at three aerosol gas flow and solution delivery rates

increase in sample input. Emission intensities from the
plasma were also slightly more stable at the 1.7 l/min argon
flow as evidenced in Figure 22. Detection limits for this
study were, therefore, all determined at an argon flow of
1.7 l/min through the aerosol chamber. With a power setting
of 25% on the ultrasonic generator, baffles in the neck of
the aerosol chamber, and an aerosol gas flow of 1.7 l/min,
the relative standard deviation of peak intensities for
repeated scans was approximately 3%.

Measured detection limits

The observed detection limits of a representative list
of elements and the lines measured are summarized in Table 7.
The site of observation giving maximal powers of detection
is also shown. The definition of a detection limit as
selected for this investigation is that concentration of
the element in solution which gives a line signal of twice
the standard deviation in background fluctuations. Solution
concentrations employed were five to ten times the extrapolated
detection limit concentrations. Amplifier gain and recorder
scale were adjusted to maximize signal-to-noise ratios while
still maintaining fluctuations in the background and a line
intensity sufficient to allow accurate measurement. Several
lines of each element were examined and the line giving the
maximum signal-to-noise ratio was utilized to calculate the
detection limit. As a general operating procedure, at least

I.I L/MIN
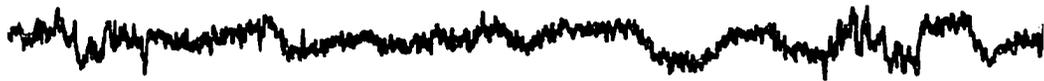
I.4 L/MIN
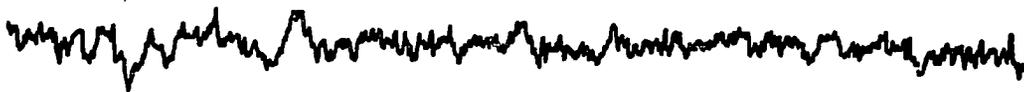
I.7 L/MIN

2.0 L/MIN

Figure 22. Observed emission stability at selected
aerosol gas flow rates

Table 7. Measured detection limits, μg/ml

Element	Wave-length Å [a]	Position (mm above load coil)	Plasma Emission	Flame Emission (23, 24, 25)	Atomic Absorption (30, 55-58)	Stabilized Arc or Plasma jet[b] (20, 21, 22)	Microwave Plasma[b] (26-29)
			Elements which form stable monoxides, $D_o(MO) > 7.0$ eV				
Ce	4186.6	25	0.007	10	95[c]	---	20
Hf	3399.8	20-30	0.01	75	15	---	---
La	4086.7	20-30	0.003	0.1(LaO)	2	---	---
Nb	4058.9	20-35	0.01	0.6	5	---	---
Ta	3012.5	20-25	0.07	18	6	---	---
Th	4019.1	25-30	0.003	150	---	---	4
Ti	3349.4	25-35	0.003	0.2	0.04[c]	0.7	1
U	4090.1	20-35	0.03	10	12	---	---
W	4008.8	20-35	0.002	0.5	3	0.8	0.2
Y	3710.3	20-25	0.0002	0.06	0.3	---	---
Zr	3438.2	15-25	0.005	3	5	---	15

[a]Wavelengths taken from reference 59. Wavelengths used were not always those used for results shown in columns 5-8.

[b]Detection limits from references 20, 21, 22, 26, 28, modified to correspond to the criterion used in this thesis.

[c]With prior desolvation of aerosol (references 55, 56).

67

Table 7. Continued

Element	Wave length Å[a]	Position (mm above load coil)	Plasma Emission	Flame Emission (23, 24, 25)	Atomic Absorption (30, 55-58)	Stabilized Arc or Plasma jet[b] (20, 21, 22)	Microwave Plasma[b] (26-29)
			Elements with excitation potentials >4.0 eV				
As	2288.1	5	0.1	6	0.2	---	4
B	2496.7	5-10	0.03	0.3(BO)	3[c]	0.05	0.03
Cd	2288.0	5-15	0.03	2	0.001	0.4	0.5
Co	3453.5	35-40	0.003	0.05	0.005	3	---
P	2136.2	5-10	0.1	3(PO)	---	1.1	---
Pb	4057.8	35-45	0.008	0.2	0.004[c]	4	1
Sb	2598.1	15-25	0.2	1.5	0.2	---	0.6
Zn	2138.6	5-10	0.009	50	0.0005[c]	0.3	0.1
			Elements with excitation potentials <4.0 eV				
Al	3961.5	30-45	0.002	0.01	0.02[c]	0.1	0.03
Ba	4554.0	20-30	0.0001	0.001	0.05	0.3	1
Cr	3578.7	25-30	0.001	0.005	0.002[c]	0.05	---
Fe	3719.9	40-45	0.005	0.05	0.002[c]	0.14	0.5
Ni	3524.5	30-50	0.006	0.03	0.005	1	0.3
Sr	4077.7	25-35	0.00002	0.0001	0.01[c]	0.07	---
V	4379.2	10-45	0.006	0.01	0.02[c]	0.2	0.1

three scans of the line and adjacent background on each side of the line were made at 5 mm intervals beginning at 5 mm and extending to 50 mm above the load coil. All elements exhibited maximum detectability at positions in the plasma below 50 mm above the load coil.

The author recognizes that detection limits are influenced by many experimental factors and that comparison of values measured by other investigators employing either similar or different analytical techniques is possible only on a semiquantitative basis. In spite of this limitation, it is instructive to compare the values with those reported in the literature for other atomic emission or absorption techniques applicable to the determination of trace elements in solution. Therefore, the lowest literature values so far reported for various other excitation sources and flame atomic absorption, including values reported with desolvated aerosols, are included in Table 7. Comparison of these values reveals superior detectability in the induction-coupled plasma for almost every element investigated.

With reference to Table 7, the powers of detection observed for those elements which tend to form exceptionally stable monoxide molecules with dissociation energies greater than 7 eV (60, 61) are of particular interest. Their observed detection limits (group 1 in Table 7) are generally 3 to 4 orders of magnitude superior to those

observed by flame atomic absorption or emission techniques.
This observation is not so surprising because the tempera-
ture and chemical environment in an argon plasma fed only
with a desolvated aerosol is far less conducive to the
formation or existence of monoxide molecules.

Another interesting comparison can be drawn for elements
whose lowest excited state is greater than 4 eV above the
ground state. These elements usually exhibit superior
detectability in flame atomic absorption as compared to
flame emission (23) because of the relatively small popula-
tion of these excited states at temperatures of 3000°K
or less. The induction-coupled plasma detection limits
for these elements (center group in Table 7) showed an
improvement of one to three orders of magnitude over flame
emission and except for Cd and Zn were equivalent to flame
atomic absorption values. The natural conclusion emerges
that the effective excitation energy in the plasma is
significantly greater than in conventional flames. Accord-
ing to a number of measurements reported in the literature
(35, 62-64), the maximum temperature prevailing in
similar Ar supported plasmas is in the 9000° to 10,000°K
range. For the plasma described in this communication,
the major portion of the sample traverses the cooler
axial channel and as a consequence the temperature experienced

by the free atoms is undoubtedly lower than 9000°K. It is clear, however, that the energy available in this channel must far exceed that prevailing in typical chemical flames.

The elements listed in the last section of Table 7 possess resonance lines with excitation potentials of approximately 4 eV or less. Detection limits for most of these elements are either equivalent or show only a moderate improvement over flame emission or absorption values. Apparently any increase in the degree of excitation of these elements is negated by their increased ionization in the plasma.

The analytical studies of Greenfield, et al. (13, 14), Wendt and Fassel (6, 15), and Hoare and Mostyn (10) have already demonstrated the relative freedom from "chemical interferences" or matrix effects on spectral line emission intensities or absorbances from these plasmas. On the other hand, Veillon and Margoshes (12), employing a 4.8 MHz plasma and a completely different aerosol introduction scheme, found surprisingly strong enhancements of calcium absorbances by increasing concentrations of phosphate or aluminum as well as other interference effects. In contrast, no interference effects up to molar ratios of 20 for the PO_4^{-3}/Ca^{+2} and 40 for the Al^{+3}/Ca^{+2} systems have been found

under the operating conditions described in this study. Preliminary studies on other interference systems have shown a similar high degree of freedom from such effects.

Determination of Impurities in Iron

Since detection limit is defined as the concentration required to produce a line intensity of only twice the fluctuations in the background intensity, an accurate quantitative determination at the detection limit concentration is not generally practical. The value of a detection limit, however, is that it provides a means of predicting a minimum quantitative determination limit. For example, if an 0.5% sample solution is to be analyzed, and if an intensity of ten times the fluctuations in the background intensity is considered as the minimum signal for an accurate quantitative determination, the minimum percentage of an impurity quantitatively measurable in the original sample is simply obtained by moving the decimal point of the detection limit, expressed in $\mu g/ml$, one position to the left.

In order to demonstrate the applicability of the induction-coupled plasma for the determination of trace constituents in a matrix material, solutions of 0.5% Fe containing trace amounts of Ce, Nb, Ti, and V were examined. These elements are often added to alloy steels and cast

irons to produce specific alloy properties (65). The
criterion presented in the previous paragraph predicts
minimum quantitative determination limits of 0.0007 wt %
for Ce, 0.001 wt % for Nb, 0.0003 wt % for Ti, and 0.0006 wt %
for V. The calibration curves obtained are illustrated in
Figure 23. Even though the most sensitive lines of Ce and
Nb could not be used because of Fe line interference, the
predicted minimum concentration for a quantitative determina-
tion was obtained for Ce. For Nb, the observed value was
only a factor of three higher than the prediction. The
determination limit for V was approximately as predicted
and for Ti was even below the predicted value. The
experimentally determined detection limit for Ti in the
presence of Fe was identical to the value in Table 7
demonstrating the absence of matrix or chemical interference
from the presence of high concentrations of Fe.

With the constricted aerosol tube positioned as
described in Table 6, the injection of the 0.5% Fe solutions
into the plasma caused deposition of solid material at the
tip of the aerosol tube. The aerosol gas flow was thus
deflected and disrupted the formation of the toroidal
shaped plasma. The problem was eliminated by positioning
the tip of the aerosol tube 1.5 cm below the top of the
inner torch tube and enlarging the injection orifice to
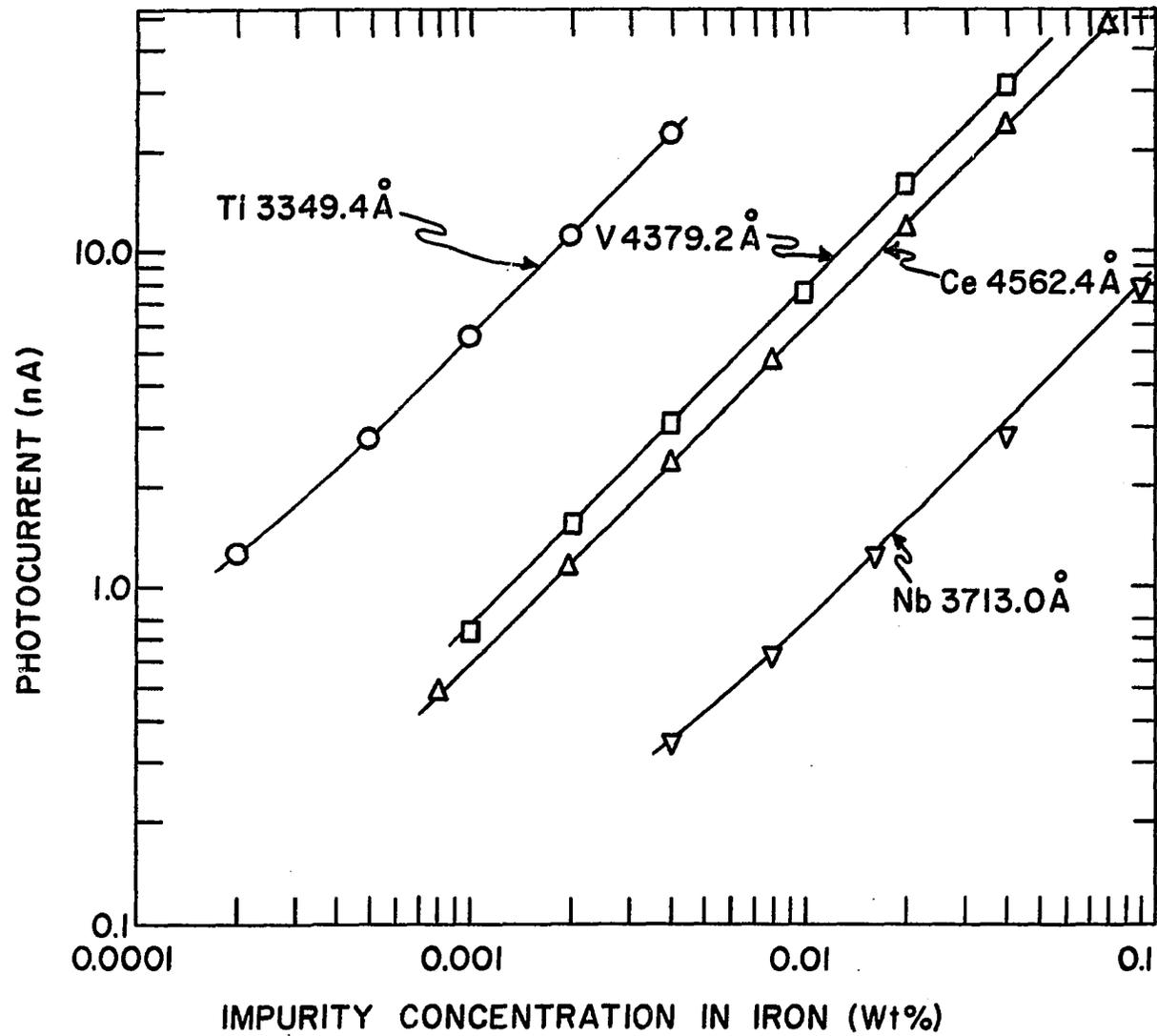2 mm i.d.

Figure 23. Experimentally determined calibration curves for four impurity elements in iron

Typical scans of the impurity element lines at
concentrations approximately in the center of the calibra-
tion curves of Figure 23 are reproduced in Figure 24.
The hump on the low wavelength side of the Ti 3349.4 $\overset{o}{A}$
peak is due to the Ti 3349.04 $\overset{o}{A}$ line. The reproducibility
of replicate scans is illustrated in Figure 25 for the Ti
3349.4 $\overset{o}{A}$ line at 0.05 µg/ml (three times the predicted
minimum determination limit concentration) in 0.5% Fe
solution. The relative standard deviation of the peak
intensities is 2.3%.

Veillon and Margoshes (12) have concluded that, except
for a few refractory elements, induction-coupled plasmas do
not appear to be a suitable replacement for chemical combus-
tion flames. This conclusion, however, was based on
observations made only under the experimental conditions
they described. In view of the superior powers of detection
and promising freedom from chemical interferences exhibited
by the plasma described in this investigation, their
deduction does not appear to be generally applicable. The
data presented herein indeed suggest that these plasmas
offer distinct advantages over combustion flames for the
emission spectrometric determination of trace elements in
solution. For almost all of the metallic elements, these
determinations can be achieved at lower concentrations than

IMPURITIES IN Fe (Wt. %)

V
4379.2 Å

Ti
3349.4 Å

Ce
4562.4 Å

Nb
3713.0 Å

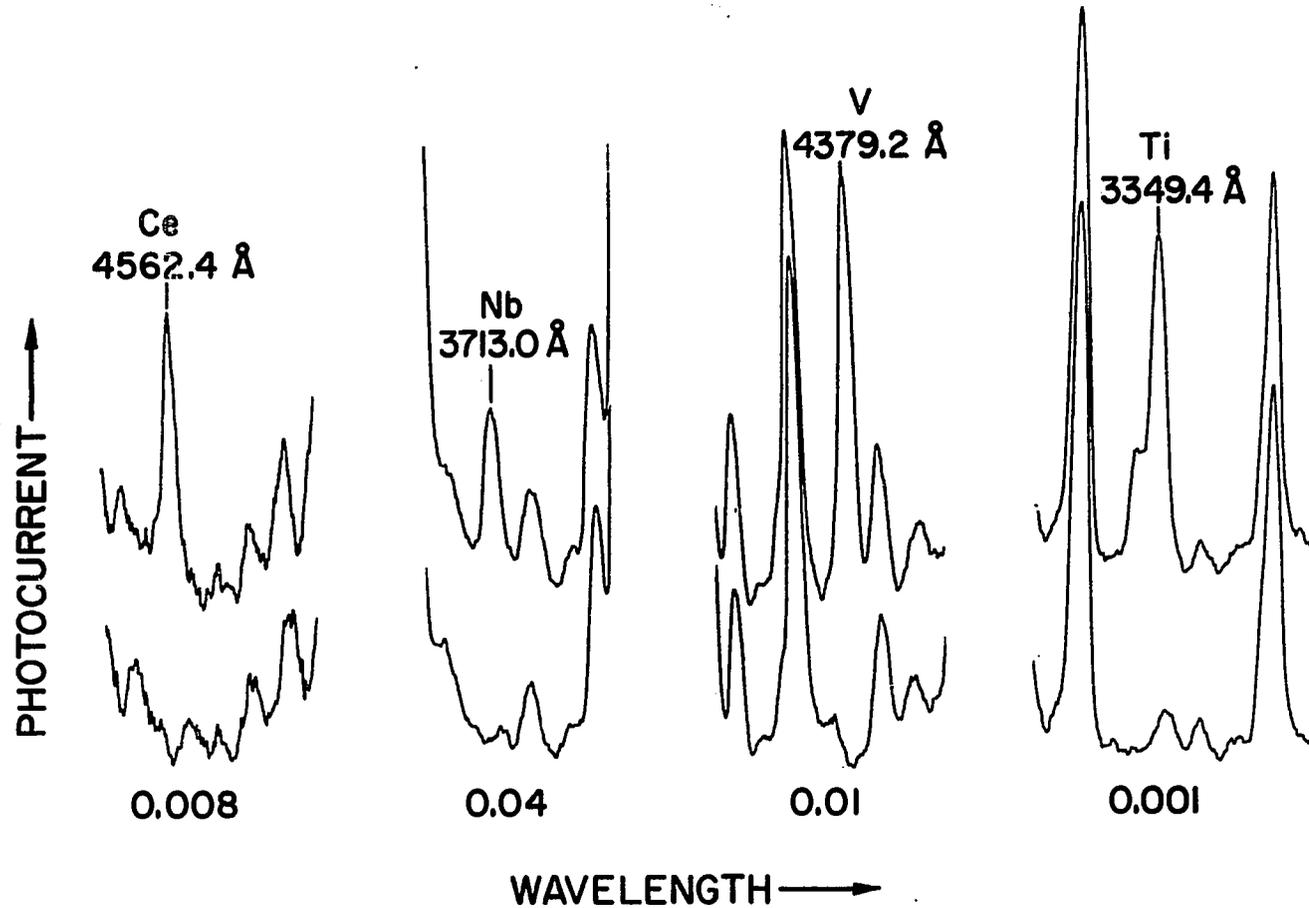PHOTOCURRENT →

WAVELENGTH →

0.008   0.04   0.01   0.001

Figure 24.   Typical scans of four impurity elements in iron at the concentra-
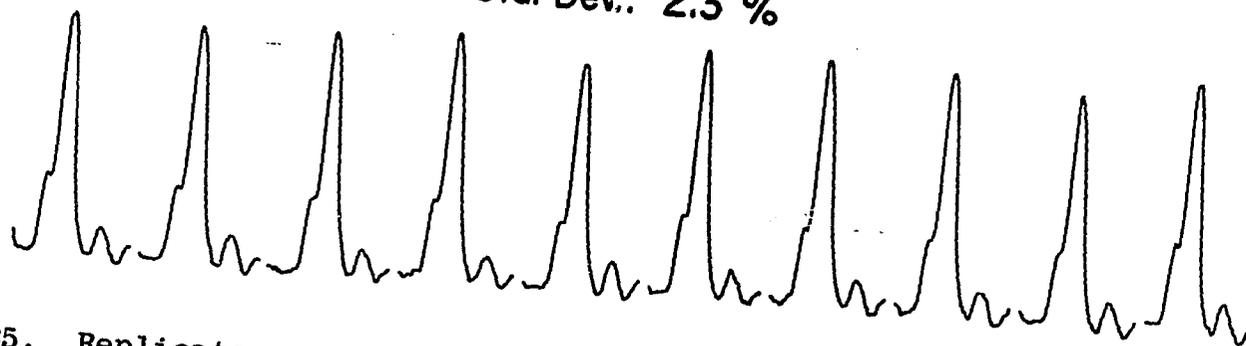tions indicated (upper) and of iron alone (lower)

Figure 25. Replicate scans of 0.05 μg/ml Ti in 0.5% Fe solution

can be realized with other spectroscopic techniques. The use of time averaged intensities from integrating detection systems should lower the minimum quantitative determination limit as well as improve the precision of analysis.

Pneumatic Nebulization

To apply the induction-coupled plasma and desolvation system to routine analysis, a means of changing sample solutions rapidly and conveniently is definitely required. In this regard, the ultrasonic nebulization facility in Figure 14 is drastically deficient. During the course of this investigation, commercial pneumatic nebulizers were developed which produce aerosol at the optimum 1.7 l/min gas flow rate as determined previously. Since these nebulizers enable rapid and convenient interchange of sample solutions, the heated chamber and the tube furnace portion of the facility illustrated in Figure 14 was redesigned to incorporate pneumatic nebulization.

A schematic diagram of the re-designed portion of the facility is shown in Figure 26. A photograph of the complete facility is shown in Figure 27. Details which apply to this facility and the operating conditions employed are listed in Table 8.

Detection limits obtained for several elements with this facility are tabulated in Table 9. Comparison of these values with the values obtained for ultrasonic nebulization also

INFRA-RED STRIP HEATER (4)

VARIABLE
PNEUMATIC
NEBULIZER

$\overline{\underline{S}}$ 24/40

HEATED CHAMBER
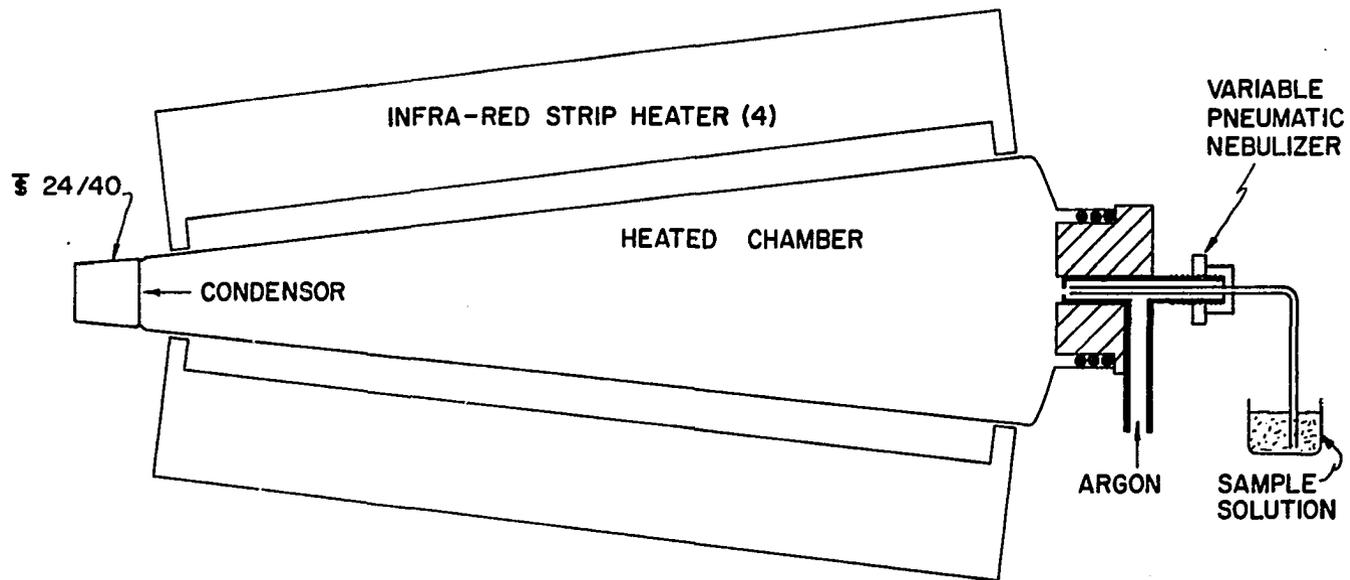
CONDENSOR

ARGON

SAMPLE
SOLUTION

79

Figure 26. Schematic diagram of pneumatic aerosol formation and desolvation
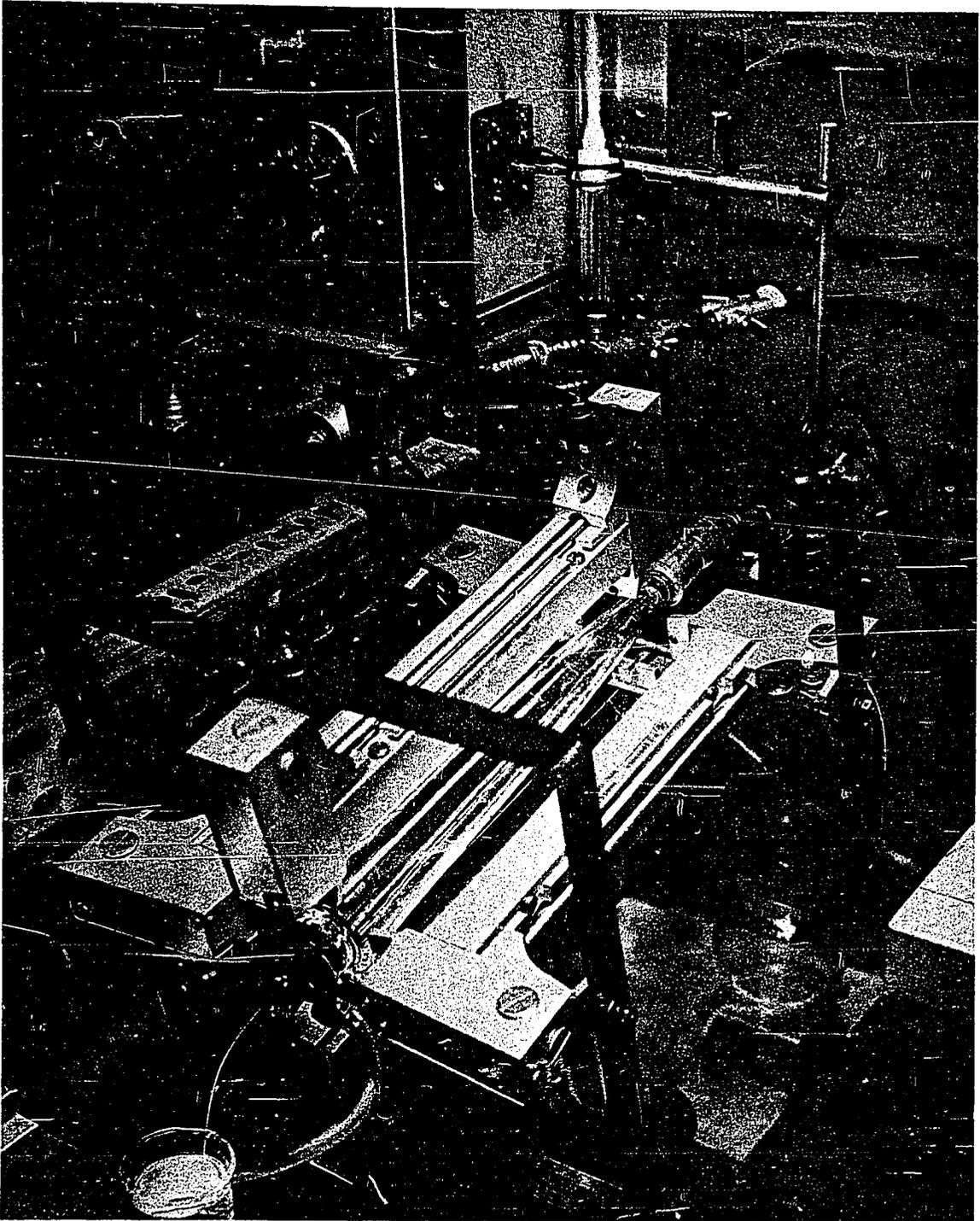facility

Figure 27. Pneumatic nebulization and desolvation facility

Table 8. Pneumatic nebulization and desolvation facilities
and operating conditions

Apparatus	Description
Nebulizer	Bausch and Lomb variable pneumatic nebulizer, part no. 33-36-13.
Heated chamber	Borosilicate glass tube 32 cm long, 4.5 cm i.d. tapered to 1.5 cm i.d. and sealed to a 𝔗 24/40 inner glass joint. A 2 cm long, 3.6 cm i.d. tube was sealed into the large end of the chamber for mounting of the nebulizer.
Heaters	4 R. I. Controls model 5305-10A parallel ray infrared strip heaters mounted at 90° intervals around the heated chamber. Each heater was operated at 100 watts output.
Nebulizer mounting piece	Nebulizer was pressed into a 3.0 cm dia. unfired lavite disk fitted with 3, 28 mm i.d. silicon o-rings. The disk was pressed into the large end of the heated chamber.
Aerosol gas flow	1.7 l/min.
Sample nebulization rate	2.4 ml/min.

Table 9.   Element detection limits, μg/ml, with pneumatic
           nebulization

Element	Pneumatic Detection limit	Ultrasonic Detection limit
Al	0.002	0.002
Ce	0.013	0.007
Th	0.003	0.003
Ti	0.002	0.003
V	0.008	0.006
Zn	0.01	0.009

included in Table 9 reveals little difference in the detecta-

bilities attainable with the two systems.   The relative

standard deviation of peak intensities for repeated scans

was 2.1 %.

The tapered heated chamber shown in Figure 26 provided

the best emission stability of several designs investigated.

The stability obtained is compared to that achieved with

the ultrasonic nebulization facility in Figure 28.   A slight

improvement in stability is apparently provided by the

pneumatic system.   However, the adjustment of the nebulization

rate to obtain this stability is very critical.   The

necessity for such a critical adjustment appears to be

directly linked to the aerosol gas flow and the design

of the heated chamber.   At some indeterminate aerosol gas

flow and solution uptake rate, the aerodynamics within the

PNEUMATIC

ULTRASONIC

Figure 28. Comparison of emission stability with
pneumatic and ultrasonic nebulization

chamber is such that a turbulence is induced, which is reflected in the plasma. The stability thus deteriorates to a level bordering on the unacceptable and readjustment of the nebulizer is required. If an aerosol gas flow rate greater than 4 l/min is employed, high stability is maintained but at a sacrifice of several orders of magnitude in emission intensity.

Even with the periodic instability, the pneumatic nebulization facility is a significant improvement over the previously described ultrasonic system. The ability to examine sample solutions in rapid succession with only minor inconvenience contributed by the sampling system should expedite the development of future applications and the execution of theoretical studies of the induction-coupled plasma.

Suggestion for Further Study

Induction-coupled plasmas are relatively new to the field of analytical spectroscopy. The theoretical investigations and analytical problems to which these plasmas could be applied are almost endless. Improved radio frequency generators for maintaining these plasmas would be a significant aid in performing future investigations. Plasma generators capable of automatically maintaining a constant optimum impedance have only recently become

commercially available. These generators should provide a facility insensitive to moderate impedance variations induced in the plasma by the introduction of sample materials. With generators of only one to two kw power output, aerosol desolvation could thus possibly be eliminated while still maintaining maximum emission intensity.

Improved nebulization techniques would also be an important contribution to future investigations. A uniform flow of aerosol should be provided with a rapid and convenient means of interchanging samples. These objectives, perhaps, may best be achieved by modification of the ultrasonic technique employed in this study. One advance in this direction is the rotating sampling device of Hoare and Mostyn (10) briefly described in the Introduction.

Studies which could be performed in the immediate future might be the determination of trace elements in various sample materials. Of particular interest should be the determination of B, P, Hf, Th, U, W, Zr, and other elements normally difficult to determine at very low concentrations by other spectroscopic techniques. Other applications could be in corrosion studies, pollution control, sea water analysis, and the analysis of high purity cooling and moderator water from nuclear reactors. The determination of inorganic constituents in various

gases such as those resulting from radioactive waste treatment and other chemical processes should be easily achieved with these plasmas. The possible detection of trace amounts of the halogens, the common gases, or elements such as S, Se, and Te may be worth investigation. Such an investigation could involve detection of the individual element or determining if molecular species of the element exist or can be produced by appropriate ma-nipulation of the plasma environment.

As previously stated, emission from the plasma appears to be free of interference effects. Although only one group of investigators has observed such effects, as mentioned in the Introduction, a very thorough study confirming the absence or existence of interference effects should be in order. A study of this nature should include a determination of the influence on emission from high concentrations of at least two types of material: elements which are readily ionizable in the plasma thereby contributing a large number of electrons and elements or molecules which form compounds with the elements under investigation that are stable at relatively high temperatures.

Atomic absorption applications with the plasma could provide another large source of study. The detection of some elements might be achieved at lower concentrations by atomic absorption than by emission. Interesting

molecular species which may exist or could be induced to exist within the plasma should be observable with spectroscopic absorption techniques. Infrared emission or absorption could possibly be employed to observe and perhaps quantitatively determine various molecular species.

Several theoretical studies could be performed with induction-coupled plasmas. Atomic absorption techniques may provide a means of observing metastable states in the plasma. Examination of their energy transfer processes and the effects these processes have on various species present in the plasma should provide an interesting study. A thorough examination of the fluid mechanical properties of the plasma could perhaps define the exact forces involved which cause the plasma to repulse sample materials. Spacial examination of various species within the plasma combined with accurate temperature maps of the plasma should answer questions as to where free atoms, ions, and molecular species are formed and why. Examination of the effect of plasma generating variables such as frequency, load coil configuration, and torch size may also provide further insight into fundamental processes occurring in the plasma.

The above areas of study represent only a few of many possible pursuits. However, this brief presentation should serve to indicate the immense potentiality of the induction-coupled plasma in analytical spectroscopy. Additional areas of possible application are explored in the next chapters.

CONTINUOUS ULTRASONIC NEBULIZATION AND SPECTROGRAPHIC ANALYSIS OF MOLTEN METALS

Historically, the spectrographic analysis of metals has been based primarily on using various electrical discharges to vaporize metal from pin or disk electrodes and to use the same discharge to excite the atomic spectra of the vaporized sample. Although remarkable speed, accuracy, and precision have been achieved, this approach has several basic limitations familiar to all emission spectroscopists. The primary limitations are the time required to take the sample and to cast, cool, and fabricate the solidified mets . into appropriate electrode forms. The direct examination of the metal in its molten state offers attractive possibilities of overcoming these limitations and of providing analyses with sufficient speed to allow continuous composition control. Several schemes for performing molten metal analysis have already been suggested (66-73). However, the problems encountered in actually performing the analysis under the high temperature and corrosive environment of a molten metal stream have not yet been resolved. In this chapter, a sampling and excitation technique which circumvents some of these basic problems is described.

Ultrasonic energy is employed to nebulize the molten metal. The finely divided aerosol quickly solidifies into a metal dust which is transported to the induction-coupled plasma by a flow of gas. In the high temperature environment of the plasma, the metal dust is vaporized and its constituents are continually excited.

Experimental Facilities

Among several schemes which can, in principle, be employed for nebulizing a molten metal (74, 75, 76), and exciting the emission spectrum of the aerosol, the simple device shown in Figure 29 has adequately demonstrated the practical feasibility of this approach.

A 20 KHz ultrasonic generator with probe assembly and amplifying step horn was used to nebulize the molten metal. When the flat tip of the step horn was brought into contact with the molten metal surface, aerosol formation occurred. In preliminary experiments with Hg, the aerosol could not be transported by a flow of gas due to coalescence of the aerosol droplets. Aerosols from higher melting point alloys solidified immediately after formation and the solidified powder was readily transportable. In the assembly shown, a 2 l/min flow of argon transported the solidified metal dust into the induction-coupled plasma. A uniform flow of nebulized woods metal into the plasma for over
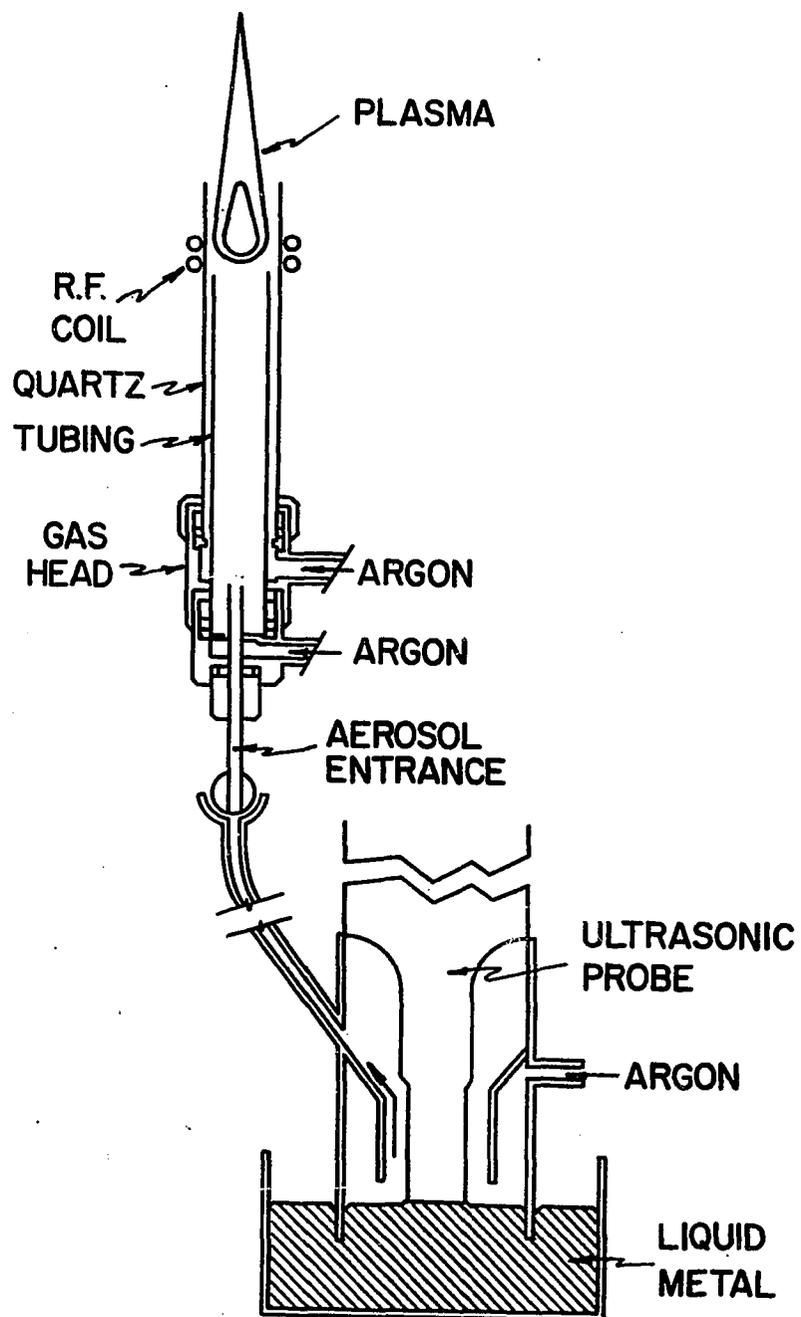
Figure 29. Ultrasonic nebulization and excitation assembly

an hour was achieved in this manner without adjustment of the liquid metal surface to the probe tip. The characteristics of this facility are listed in Table 10.

For the early exploratory experiments involving observations on the nebulization and excitation of Woods metal, a Jarrell-Ash Model 82000, 0.5-meter Ebert mounting scanning spectrometer was used. The detection system was that described in Table 5. The 1-meter Czerny-Turner mounting, scanning spectrometer described in Table 4 with a photographic attachment was employed for the quantitative analytical calibrations. Kodak SA no. 1 plates were used to photograph the spectra. Microphotometry and intensity ratio calculations followed standard practices (77).

During this concurrent study with solutions, the plasma was first transformed into the toroidal shape. However, since maximum intensity was not a goal of this study and the intensity from the toroidal shaped plasma made very short exposure periods necessary, the uniform shaped plasma was utilized. In this manner, reasonable exposure periods of 15 to 30 seconds could be employed.

Results and Discussion

No difficulties were encountered in reproducing spectral intensity ratios when molten Woods metal - an alloy of bismuth (50%), lead (25%), cadmium (12.5%) and tin (12.5%),with 75°C melting point - was examined. For this alloy 21 repeated

Table 10. Molten metal nebulization facilities and
          operating conditions

Apparatus	Description
Aerosol generator	Bronwill Scientific, Biosonik - II high intensity ultrasonic probe, 125 watts nominal output, 20 KHz frequency.
Aerosol delivery tube and gas flow	Borosilicate glass, 5 mm i.d., 7 mm o.d., terminating at bottom of plasma tube. A flow of 2.0 l/min Ar was used to transport the solidified aerosol to the plasma.
Standard samples	Morris P. Kirk and Sons, Inc., tin-base solder - Standard Numbers 583-87, 584-69, 585-75, P939-14, P940-13, and P941-13.

scans of the Sn 3034.1 $\overset{o}{A}$ and Bi 3024.6 $\overset{o}{A}$ lines over a period

of one hour gave a relative standard deviation of 4.9% for

the Sn 3034.1 $\overset{o}{A}$/Bi 3024.6 $\overset{o}{A}$ intensity ratio. When higher

melting point alloys were examined, the probe assembly

tended to overheat during continuous nebulization periods

exceeding 15 minutes. These observations suggest that inter-

mittent on-off operation - for periods on the order of 15 to

30 seconds - may be necessary in some applications. This

mode of operation presents no problems when integrating-type,

direct-reading spectrometers are employed for quantitative

measurements of intensity ratios, because integration periods

of this magnitude are commonly used.

With the present spectroscopic experimental facilities, quantitative intensity ratio measurements could only be performed by photoelectric, spectral-scanning techniques or by photographic recording of the spectra. Since the spectral-scanning approach required continuous nebulization periods longer than 15 minutes when the spectral lines of interest covered a wide wavelength region, recourse was taken to photographic recording for most of the quantitative experiments.

In order to demonstrate the applicability of the ultrasonic nebulization technique to the quantitative determination of constituents in a molten alloy, a series of tin-base solder standard samples (listed in Table 10) were examined. The melting points of these alloys were 190 ± 10°C. The exposure periods for this alloy varied from 20 to 30 seconds. The analytical curves shown in Figures 30 and 31 are typical of those obtained for the impurities in the series of standards examined. The relative standard deviations for ten observations at each of the concentrations plotted in the figures were 6.1% and 12.2%, respectively, for copper and arsenic.

For the tin-base solder alloys, Stoke's law calculations showed that solidified particles with a maximum diameter of 12 to 14 μ should be transported to the plasma by the 2 l/min argon flow. These predictions were confirmed by
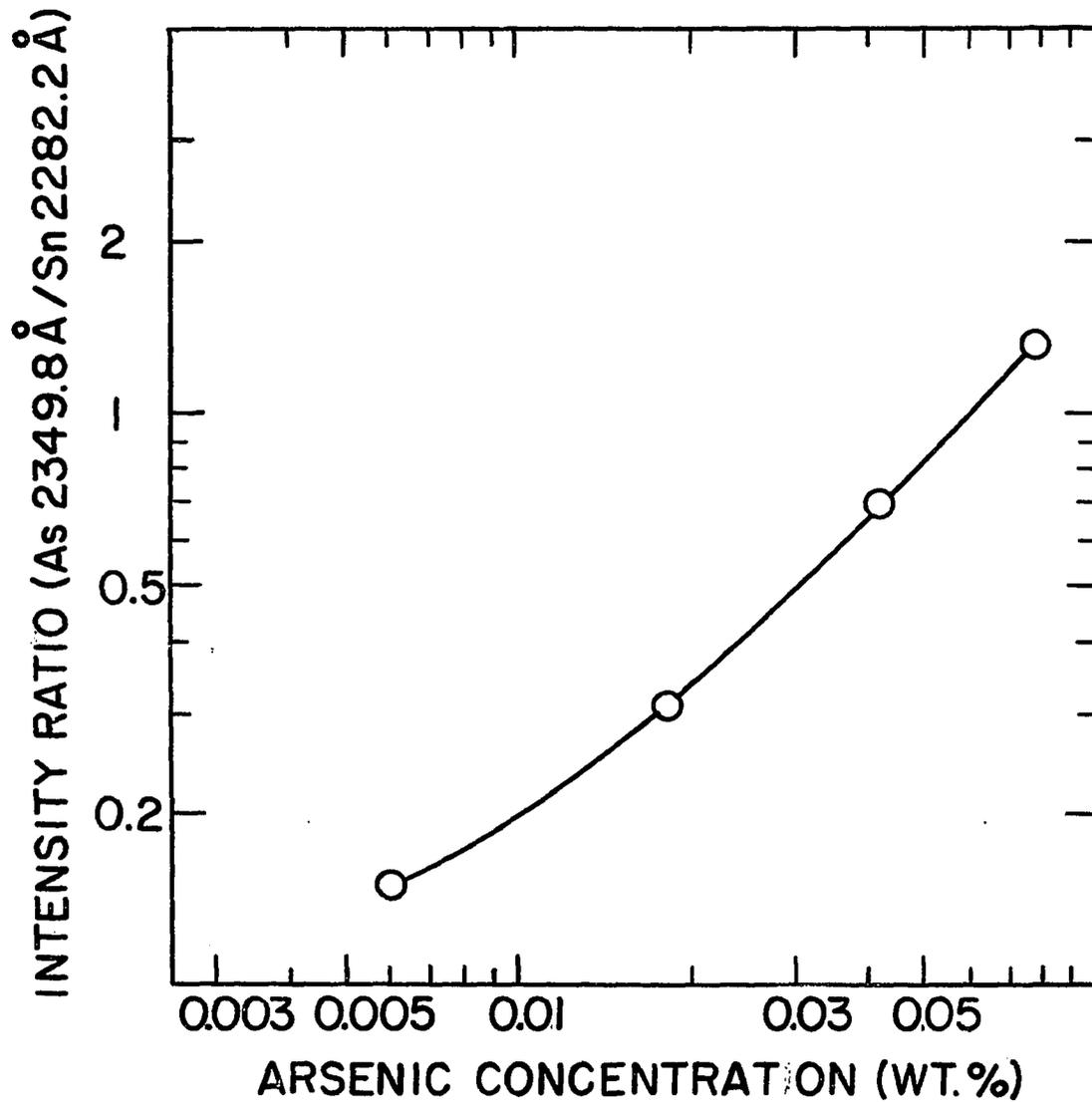
Figure 30. Analytical curve for the determination of arsenic in tin-base solder
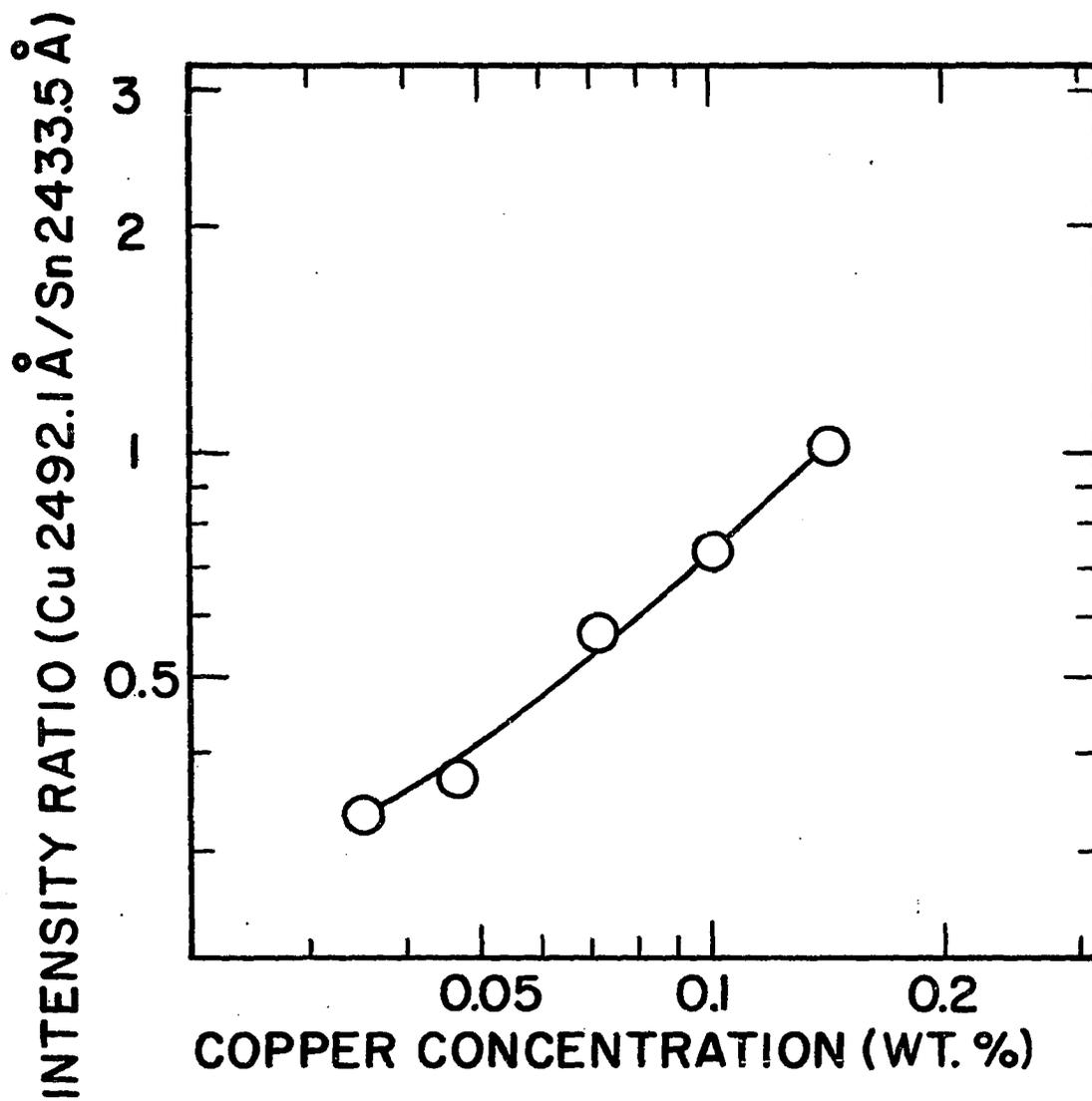
Figure 31. Analytical curve for the determination of copper
in tin-base solder

direct measurement of particle size distribution. A photo

of the particles obtained is shown in Figure 32. The

majority of particles are 12 μ or less in diameter, and

the largest particles observable are in the 14 to 15 μ diameter

range. Undoubtedly, larger aerosol particles were produced

but were not transported to the plasma by the gas flow

employed. The flow of powdered aerosol to the plasma was

not determined, but was estimated to be in the 1-10 mg/min

range.

Suggestions for Further Study

The above results demonstrate that continuous composition

monitoring of molten metals in either static or flowing systems

is now in the realm of possiblity and suggests several areas

of investigation. With appropriate adaptations of this or

other ultrasonic nebulization techniques, high melting

point metals should be equally amenable to analysis in the

induction-coupled plasma. These metals may require the use of

relatively long plasmas to provide sufficiently long residence

times within the plasma to insure complete vaporization of

the solidified aerosol. Long plasmas could possibly be

obtained with long solenoid inductors and generators of

higher power capabilities than the one available for this

study. Another scheme for molten metal sampling might be

the use of a high powered laser to flash vaporize a portion

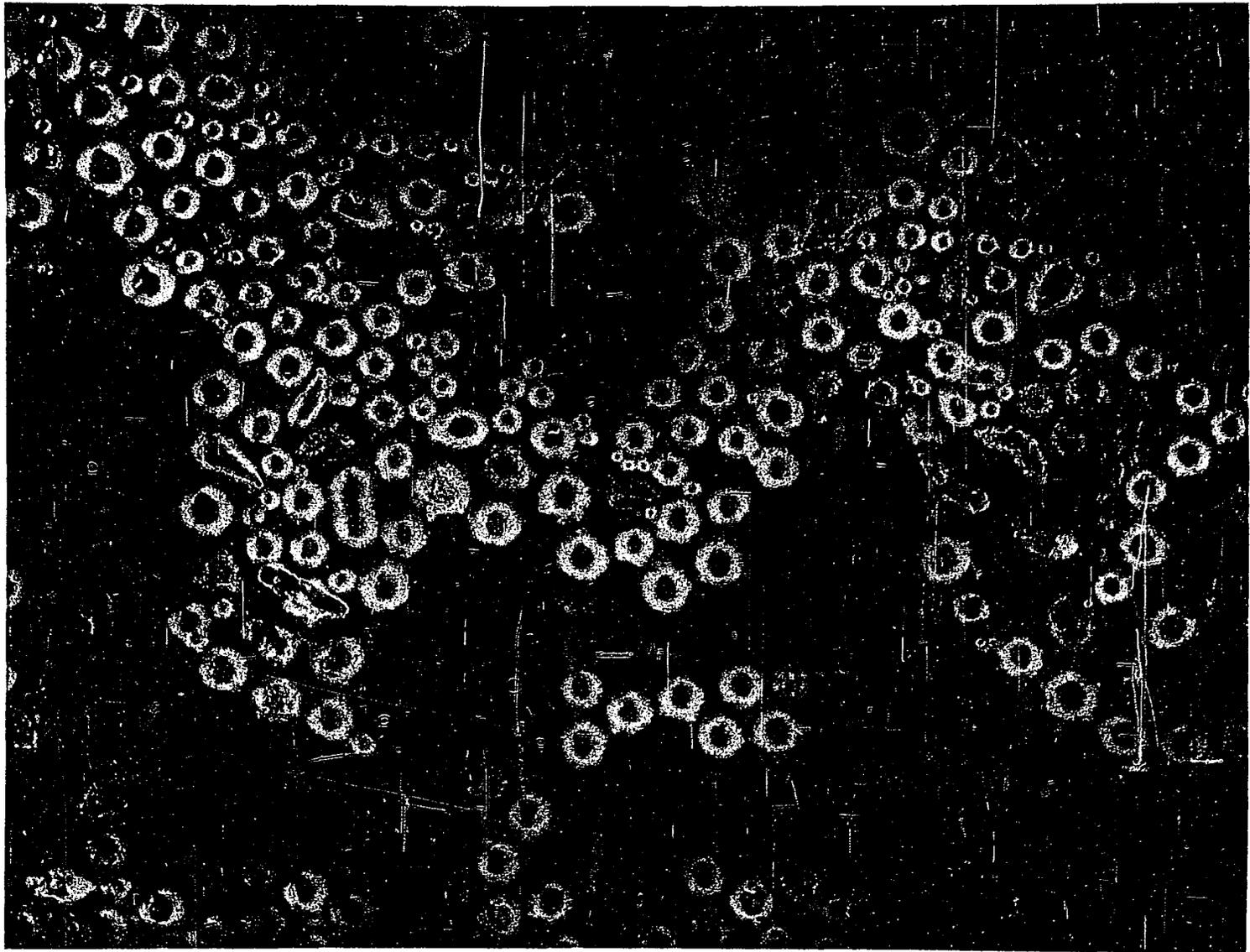of the melt surface. The resulting vapor should be readily

Figure 32. Photomicrograph of solidified aerosol from ultrasonically nebulized molten Sn-Pb alloy

transportable to an induction-coupled plasma. Other materials in liquid form such as oils, paints, molten plastics, biological fluids, and various process liquors should also be amenable to continous analysis by ultrasonic nebulization and plasma excitation techniques.

The aerosol from ultrasonically nebulized molten metal is a powder consisting of spherical particles. A process for the production of micron sized spheroids of metals is thus indicated which is perhaps also worth further investigation.

OBSERVATIONS ON THE INTRODUCTION OF POWDERS
INTO THE PLASMA

The quantitative spectrographic analysis of powder materials is generally accomplished in one of two ways: (1) the sample is dissolved and the resulting solution analyzed by flame atomic emission or absorption techniques or by excitation of the atomic spectra in an electrical discharge; or (2) the sample is mixed with appropriate materials, pressed into an electrode, and then vaporized and the atomic spectra excited by an electrical discharge. Both of these techniques require considerable time and effort to prepare each sample for analysis. The direct examination of powdered samples could possibly eliminate this need for sample preparation. The ability to transport powders with a flowing gas stream offers a particularly attractive means of introducing powdered samples into an induction-coupled plasma for direct examination. Hoare and Mostyn (10) were the first to report the direct analysis of powders employing induction-coupled plasma excitation. Concurrent with the investigations discussed in previous chapters, several powdered materials were introduced into the plasma. Although no attempt was made to develop analytical capabilities, several interesting observations

were made.

Powder Transport Devices

Three devices used to transport powder from a reservoir in a continuous flow are the aspiration, aeration, and auger type powder feed units. In the aspiration type, powder is forced through a small orifice in the bottom of the powder reservoir by a high velocity flow of gas (see Figure 33). Ideally, the aspirated powder is continually replaced from the reservoir resulting in a continuous flow of powder through the orifice. The flow of powder is then transported through a tube to any desired location. In an aeration powder feed unit (see Figure 34), a flow of gas passing vertically upwards through the powder in the reservoir carries a portion of the powder to an outlet positioned above the surface level of the powder. The aerated powder is also transported from the reservoir through a tube by the flow of gas. In both the aeration and aspiration units, the flow of gas frequently forms channels through the powder. The gas flowing through these channels no longer entrains powder which, accordingly, results in a reduction in the flow of powder from the reservoir. Channeling is generally prevented by inducing vibrations in the powder with a mechanical vibrator attached to the powder reservoir. The

SAMPLE
CANISTER

PRESSURE
RELIEF
TUBE

SAMPLE POWDER

CARRIER
GAS
+
PWD
SAMPLE
OUT
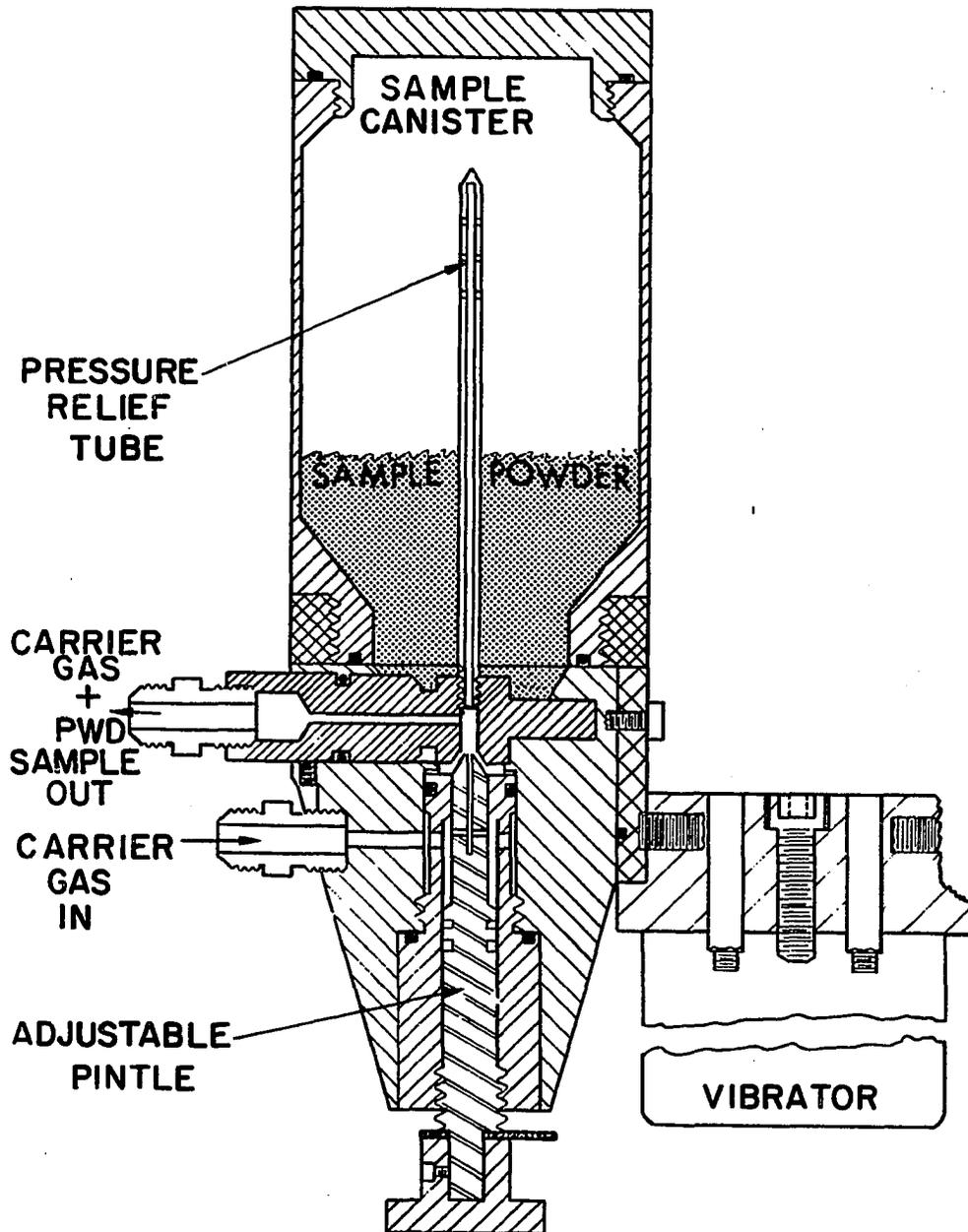
CARRIER
GAS
IN

ADJUSTABLE
PINTLE

VIBRATOR

Figure 33.   Schematic diagram of commercial aspiration
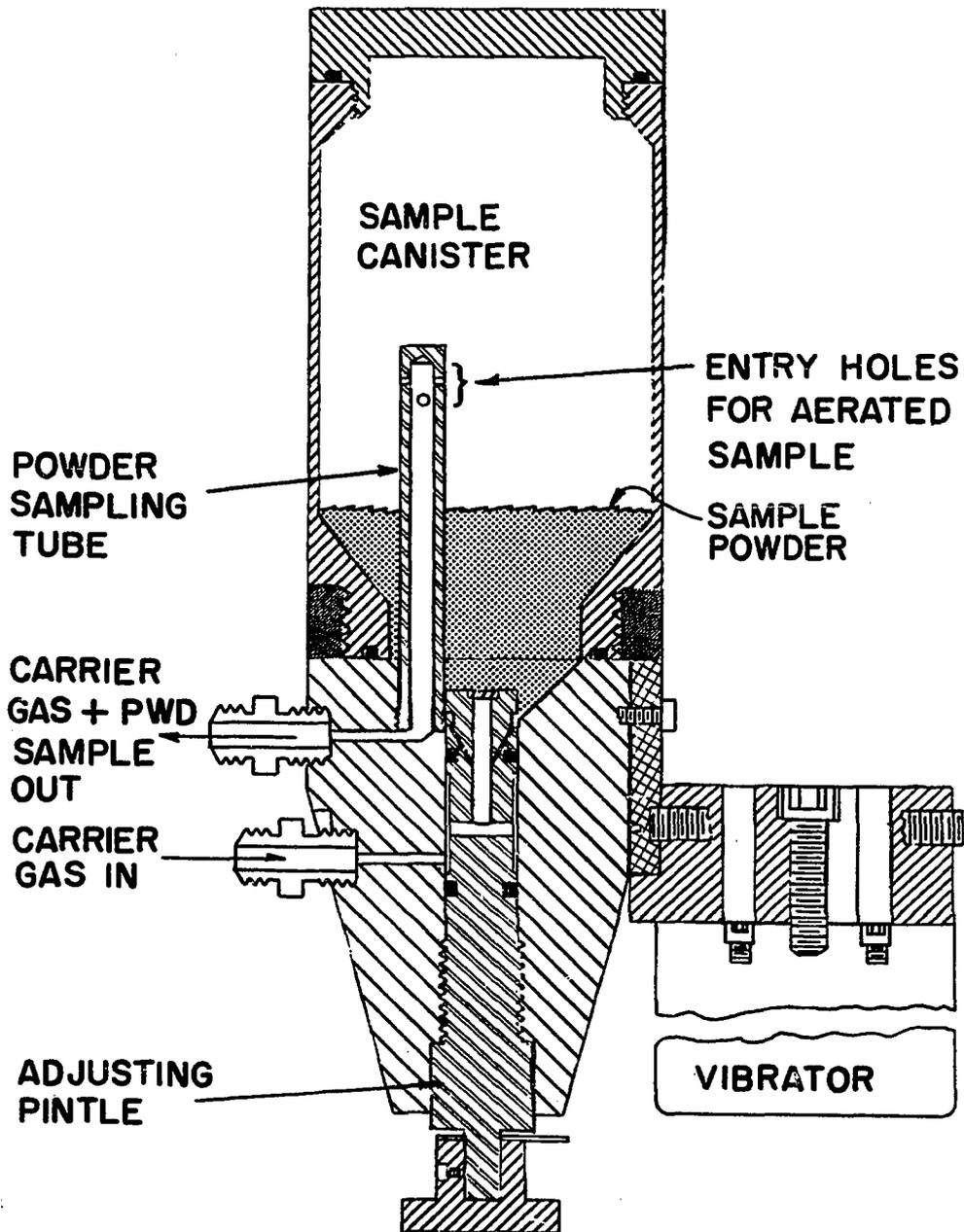powder feed unit

Figure 34. Schematic diagram of commercial aeration
powder feed unit

auger powder feed unit is simply a screw auger with one end in the bottom of the powder reservoir and the other at the desired delivery site.

For accurate quantitative analysis of powdered samples by induction-coupled plasma excitation, the following requirements should be met: (a) the flow of powder to the plasma should be uniform, particularly if photoelectric observation is employed; (b) sufficient powder should be supplied to the plasma to permit trace element detection; and (c) the powder should be completely vaporized in the plasma.

In this investigation, the aspiration and aeration type units were employed. These included a commercial unit of each type and one aeration unit designed by the author. The commercial aspiration and aeration units were both from Humphry's Corporation, Tafa Division, model numbers 101 and 102 respectively and are shown in Figures 33 and 34. The plasma torch was operated in the inverted position and the powder introduced into the plasma from above.

Observations

The commercial powder feed units were both used to introduce powders of Al_2O_3, $Li_2B_4O_7$, and Al metal into the plasma. Both units could deliver up to 10 mg/min of powder to the plasma, however; the adjustment of powder flow was difficult, particularly for the aspiration unit. The

$Li_2B_4O_7$ particles were less than 5 μ in diameter and were completely vaporized in the plasma. The Al_2O_3 and Al metal were less than 50 μ in diameter and unvaporized particles were observed passing through the plasma. These particles were also observed being reflected from a uniform shaped plasma. Consequently, the particles must be less than 50 μ in diameter for complete vaporization to occur and can probably be as large as 15 μ in diameter. The flow of powder from the aeration unit was considerably more uniform than from the aspiration unit and the emission intensity was accordingly more stable. However, as seen in Figures 33 and 34, both units have a 90° bend in the powder outlet. The powder thus had to pass through a section of horizontal tubing in which a portion of the powder deposited. After a few minutes operation, some of the accumulated powder was periodically transported to the plasma and caused bursts of emission which precluded the measurement of emission intensities.

A simple aeration powder feed unit with the outlet directly into the plasma was thus designed and is shown in Figure 35. The unit was constructed from a sealing tube of borosilicate glass. A photograph of the unit in position is shown in Figure 12. The rate at which powder is delivered from the aeration unit to the plasma is controlled by density, particle size, and gas flow according to Stoke's
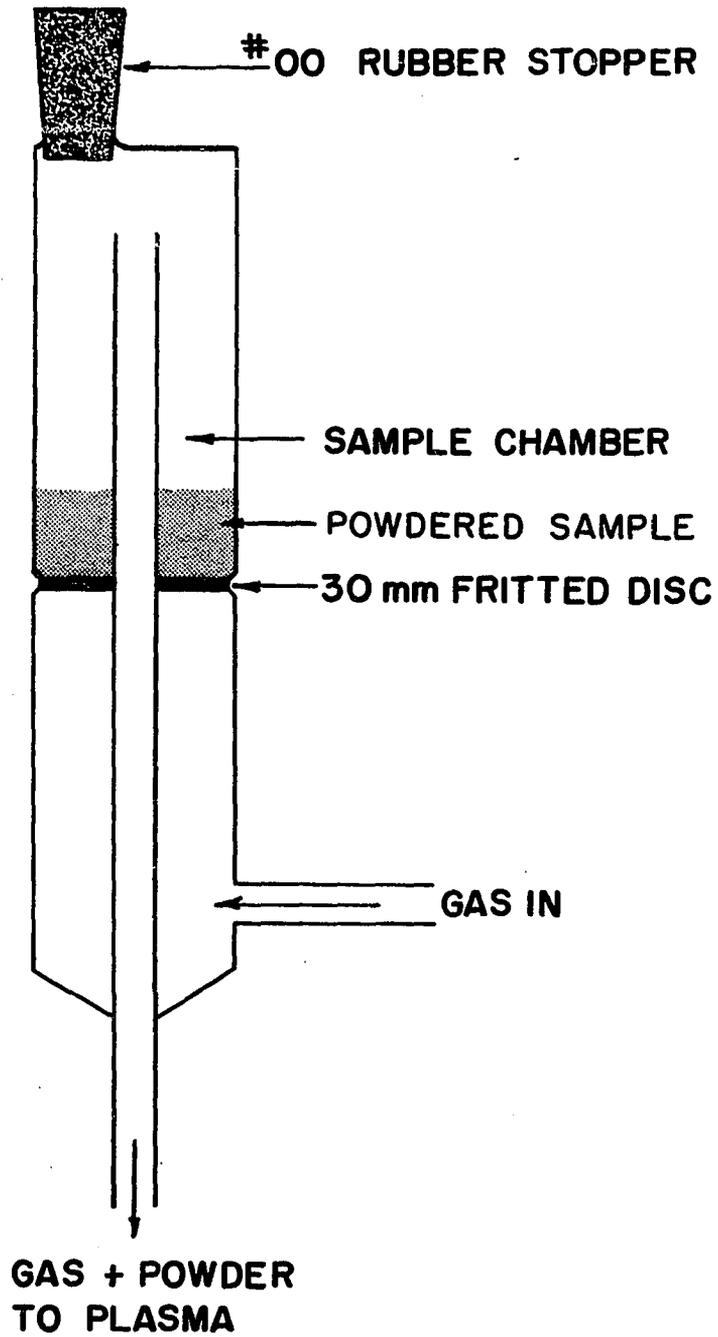
Figure 35. Aeration powder feed unit

law. When powders having a relatively wide particle size distribution were examined, the emission intensity gradually decreased because of depletion of the smaller particles in the powder feed unit. Thus, in order to obtain a uniform flow of powder, the size of the powder particles had to be nearly uniform and small enough to be carried by the flow of gas employed. The powder also had to be free of moisture or compaction occurred.

An indication of the stability of the powder introduction system and the sensitivity attainable for rare earth elements was obtained by examination of a sample of Y_2O_3 containing known amounts of Dy, Er, Gd, Ho, and Yb. The sample was ground to a particle size of less than 15 μ in diameter and introduced into the plasma at a rate of approximately 5 mg/min with an argon flow of 2 l/min. The sample was completely vaporized in the plasma. All of the impurity elements were detected and the concentrations and lines observed are listed in Table 11. The relative standard deviation of the Dy/Y ratio for replicate scans of the Dy 4211.7 $\overset{o}{A}$ line and the Y 4217.8 $\overset{o}{A}$ line was 9.3%.

<div align="center">Suggestions for Further Study</div>

This brief investigation and the results of Hoare and Mostyn (10) demonstrate that powdered samples can be analyzed directly in an induction-coupled plasma. The

Table 11. Impurities in Y_2O_3 sample

Element	Wavelength A	Concentration µg/g
Dy	4211.7	2090
Er	3906.3	104
Gd	3768.4	1040
Ho	3456.0	260
Yb	3694.2	530

ability to detect less than 100 µg/g of Er impurity in a Y_2O_3 powder suggests a sensitive technique for the determination of rare earths in various materials. However, if time consuming sample preparation procedures are to be avoided, improved sample introduction techniques and plasmas capable of vaporizing relatively large particles are needed. The improved plasma generators and long plasmas discussed in the previous chapter should be a significant aid in the development of future applications to the direct analysis of powdered materials. Applications of immediate interest which could probably be performed with present sample introduction techniques could be the analysis of ion-exchange microspheres and the continuous monitoring of impurity constituents in powders from production processes.

DISCUSSION

The results of this investigation have demonstrated the vast potential of induction-coupled plasmas as sources for analytical spectroscopy. The guidelines established for the development of a versatile plasma generating facility have provided an ability to determine trace elements in solution at concentrations lower than can be determined by other spectroscopic techniques. These superior powers of detection and the promising freedom from chemical interferences presage an increase in the application of these plasmas to the determination of trace elements in solution. Of particular interest in comparison to combustion flames are the four to five orders of magnitude improvement provided by the relatively oxygen free plasma in the detectability of those elements which form stable monoxide molecules: notably, Ce, Ta, Hf, Th, U, and Zr. The ultrasonic technique developed for the nebulization of molten metals and induction-coupled plasma excitation of the resulting aerosol provides a unique scheme for the direct analysis of metals in the molten state. With appropriate adaptation of this or other ultrasonic nebulization techniques, continuous composition monitoring of molten metal streams is now in the realm of possibility. Powdered materials can be introduced into the plasma, vaporized, and the

atomic spectra excited. Thus, the direct analysis of powder samples is possible. Several areas of application for the induction-coupled plasma have been presented in Suggestions for Future Study in the previous chapters. These areas obviously represent only a few of the possibilities for this versatile spectral source.

The plasma, however, is not without some disadvantages. In comparison to combustion flames the equipment and operating cost is more expensive. However, these expenses are less than for arc and spark sources. The spectra from elements introduced into the plasma are more complex than from combustion flames which makes the use of spectrometers with higher resolution desirable. Before the plasma can be readily adapted to routine analytical systems, improvements in sampling techniques which provide rapid and convenient interchange of samples are needed.

The recent appearance of compact, constant impedance plasma generators and the increasing interest of practicing spectroscopists in ultrasonic nebulization techniques should diminish these disadvantages. The future application of the induction-coupled plasma in analytical spectroscopy indeed appears promising.

LITERATURE CITED

1. Scholz, P. D. An electrical-thermal study of the RF induction coupled plasma torch. Unpublished M.S. thesis. Evanston, Ill., library, Northwestern University. 1965.

2. Reed, T. B. Induction-coupled plasma torch. Journal of Applied Physics 32: 821. 1961.

3. Mironer, A. and H. Hushfar. Radio frequency heating of a dense, moving plasma: Preprint 63045-63. Unpublished paper presented at AIAA Electric Propustion Conference, Colorado Springs, Colo., March, 1963. American Institute of Aeronautics and Astronautics, New York, New York. Ca. 1963.

4. Babat, G. I. Electrodeless discharges and some allied problems. Institute of Electrical Engineering (London) Journal 94; Part 3: 27. 1947.

5. Reed, T. B. Plasma torches. International Science and Technology 6: 42. June 1962.

6. Wendt, R. H. and V. A. Fassel. Induction-coupled plasma spectrometric excitation source. Analytical Chemistry 37: 920. 1965.

7. Reed, T. B. Growth of refractory crystals using the induction plasma torch. Journal of Applied Physics. 32: 2534. 1961.

8. Wendt, R. H. Spectroscopic properties and analytical applications of induction-coupled plasmas. Unpublished Ph.D. thesis. Ames, Iowa, library, Iowa State University. 1965.

9. Greenfield, S., I. Ll. Jones and C. T. Berry. High-pressure plasma as spectroscopic emission sources. Analyst 89: 713. 1964.

10. Hoare, H. C. and R. A. Mostyn. Emission spectrometry of solutions and powders with a high-frequency plasma source. Analytical Chemistry 39: 1153. 1967.

11. Britske, M. E., V. M. Borisov and Yu. S. Sukach. Electrodeless high-frequency discharge with axial aerosol flow as a light source for spectral analysis. Industrial Laboratory (translation of Zavodskaya Laboratoriya) 33, No. 2: 301. 1967.

12. Veillon, C. and M. Margoshes. An evaluation of the induction—coupled, radio-frequency plasma torch for atomic emission and atomic absorption spectrometry. Spectrochimica Acta 23B: 503. 1968.

13. Greenfield, S., I. Ll. Jones, C. T. Berry, and L. G. Bunch. The high frequency torch: some facts, figures, and thoughts. Analytical Chemistry Society Proceedings 2: 111. 1965.

14. Greenfield, S., C. T. Berry, and L. G. Bunch. Spectroscopy with a high frequency plasma torch. Des Plaines, Ill., Radyne International, Inc., ca. 1966.

15. Wendt, R. H. and V. A. Fassel. Atomic absorption spectroscopy with induction-coupled plasmas. Analytical Chemistry 38: 337. 1966.

16. Fassel, V. A. and G. W. Dickinson. Continuous ultrasonic nebulization and spectrographic analysis of molten metals. Analytical Chemistry 40: 247. 1968.

17. Barnett, W. B. A theoretical and experimental study of internal standardization in analytical emission spectroscopy. Unpublished Ph.D. thesis. Ames, Iowa, Library, Iowa State University. 1968.

18. Barnett, W. B., V. A. Fassel and R. N. Kniseley. Theoretical principles of internal standardization in analytical emission spectroscopy. Spectrochimica Acta 23B: 643. 1968.

19. Veillon, C. and M. Margoshes. A pneumatic solution nebulization system producing dry aerosol for spectroscopy. Spectrochimica Acta 23B: 553. 1968.

20. DeKalb, E. L., R. N. Kniseley and V. A. Fassel. Optical emission spectroscopy as an analytical tool. New York Academy of Sciences Annals 137, Article 1: 235. January 20, 1966.

21. Marinković, M. and B. Dimitrijević. Low-temperature arc as a light source for emission spectrometric analysis of solutions. Spectrochimica Acta 23B: 257. 1968.

22. Goto, H. and I. Atsuya. Fundamental studies on plasma-jet spectrometry. Zeitschrift für Analytische Chemie 225: 121. 1967.

23. Fassel, V. A. and D. W. Golightly. Detection limits of elements in the spectra of premixed, oxy-acetylene flames. Analytical Chemistry 39: 446. 1967.

24. Pickett, E. E. and S. R. Koirtyohann. The nitrous oxide-acetylene flame in emission analysis--I. General characteristics. Spectrochimica Acta 23B: 235. 1968.

25. Koirtyohann, S. R. and E. E. Pickett. The nitrous oxide-acetylene flame in emission analysis - II. Lithium and the alkaline earths. Spectrochimica Acta 23B: 673. 1968.

26. Goto, H., K. Hirokawa and M. Suzuki. Spectrometric determination of various metals by high-frequency plasma torch. Zeitschrift fur Analytische Chemie 225: 130. 1967.

27. Murayama, S., M. Hiromitsu and M. Yamamoto. Excitation of solutions in a 2450 MHz discharge. Spectrochimica Acta 23B: 513. 1968.

28. Pforr, G. and K. Langner. Quantitative analysis of aqueous solutions by ultrasonic dispersion and excitation by torch discharge. Zeitschrift fur Chemie 5: 115. 1965.

29. Pforr, G. and V. Kapicha. Zur temperatur einer fackelentladung fur die losungs spektralanalyse. Collection of Czechosolvak Chemical Communications 31: 4710. 1966.

30. Slavin, W. Atomic absorption spectroscopy. Interscience Publishers, New York, N.Y., 1968.

31. Brown, G. H., C. N. Hoyler, and R. A. Bierwirth. Theory and application of radio-frequency heating. D. Van Nostrand Co., Inc., New York, N.Y., 1947.

32. Langton, L. L. Radio-frequency heating equipment.
    Pitman Publishing Corporation, New York, N.Y. 1949.

33. May, E. Industrial high frequency electric power.
    John Wiley and Sons, Inc., New York, N.Y., 1950.

34. Marynowski, C. W. and A. G. Monroe. Discussion of r-f
    generation of thermal plasmas. International Symposium
    on High Temperature Technology Proceedings 1963:
    525. 1964.

35. Hughes, D. W. and E. R. Wooding. The temperature
    distribution in an h-mode r-f plasma torch. Physics
    Letters 24A: 70. 1967.

36. Marynowski, C. W. and A. G. Monroe. R. F. generation
    of thermal plasmas. International Symposium on High
    Temperature Technology Proceedings 1963: 67. 1964.

37. Kana'an, A. S. Studies at high temperatures.
    Unpublished Ph.D. thesis. Madison, Wisc., Library,
    University of Wisconsin. 1963.

38. Beguin, C. P., J. B. Ezell, A. Salzemini, J. C.
    Thompson, D. G. Vickroy, and J. L. Margrave. Chemical
    syntheses in radio-frequency plasma torches. In R. F.
    Baddour and R. S. Timmins, ed. The application of
    plasmas to chemical processing. Pp. 35-53. Cambridge,
    Mass., The M.I.T. Press. 1967.

39. Terman, F. E. Electronic and radio engineering.
    4th ed. McGraw Hill, New York, N.Y., 1955.

40. Riemann, M. Ein stabilesierter Lichtbogen für die
    Lösungsspektralanalyse. In Ritschl, R. and G. Holdt,
    eds. Emissionsspektroskopie. Pp. 173-180. Akademie -
    Verlag, Berlin, Germany. 1964.

41. Woodriff, R. Resistance to the introduction of solids
    and liquids into high energy spectroscopic sources.
    Applied Spectroscopy 22: 207. 1968.

42. West, C. D. and D. N. Hume. Radiofrequency plasma
    emission spectrophotometer. Analytical Chemistry 36:
    412. 1964.

43. Dunken, H., G. Pforr, W. Mikkeleit, and K. Geller.
    Fremdenergierstäubung in der Flammenphotometrie.
    Spectrochimica Acta 20: 1531. 1964.

44. Kirsten, W. J. and G. O. B. Bertisson. Direct continuous quantitative ultrasonic nebulizer for flame photometry and flame absorption spectroscopy. Analytical Chemistry 38: 648. 1966.

45. Hoare, H. C., R. A. Mostyn, and T. B. Newland. An ultrasonic atomiser applied to atomic absorption spectrophotometry. Analytica Chemica Acta 40: 181. 1968.

46. Owen, L. E. Investigation of techniques for the introduction of liquid samples into a plasma arc for alloy analysis. Air Force Materials Laboratory and Technology Division Report AFML - TR - 67 - 400 [Air Force Systems Command Wright-Patterson Air Force Base, Ohio. 1968.

47. Robert, M. E. Applications des ultrasons a la dispersion des solutions en absorption atomique. Méthodes Physiques D'Analyse 4: 231. 1968.

48. Spitz, J. and G. Uny. La pulvérisation par ultra-sons appliqueé a la spectrométrie d'absorption atomique. Applied Optics 7: 1345. 1968.

49. West, C. D. Ultrasonic sprayer for atomic emission and absorption spectrochemistry. Analytical Chemistry 40: 253. 1968.

50. Mermet, J. M. and J. P. Robin. Ultrasonic nebulizer for easily changing sample solutions. Analytical Chemistry 40: 1918. 1968.

51. Rayleigh, J. W. S. Tne theory of sound. Vol. 2. Dover Publications, New York, N.Y. 1945.

52. Lang, R. J. Ultrasonic atomization of liquids. Acoustical Society of America Journal 34: 6. 1962.

53. Peskin, R. L. and R. J. Raco. Ultrasonic atomization of liquids. Acoustical Society of America Journal 35: 1378. 1963.

54. Dubbs, C. A. Increased sensitivity for the Perkin-Elmer flame photometer. Analytical Chemistry 24. 1654. 1952.

55. Venghiattis, A. A. A heated chamber burner for atomic absorption spectroscopy. Applied Optics 7: 1313. 1968.

56. Hell, A., W. F. Ulrich, N. Sutin, J. Ramirez-Munoz.
    Laminar flow burner system with infrared heated spray
    chamber and condensor. Applied Optics 7: 317. 1968.

57. Fiorino, J. A., R. N. Kniseley, and V. A. Fassel.
    A versatile long-path, slot burner for atomic absorp-
    tion spectroscopy with oxyacetylene and nitrous oxide-
    acetylene flames. Spectrochimica Acta 23B: 413.
    1968.

58. Koirtyohann, S. R. Recent developments in atomic
    absorption and emission spectroscopy. Atomic
    Absorption Newsletter 6, No. 4: 77. 1967.

59. Meggers, W. F., C. H. Corliss, and B. F. Scribner.
    Tables of spectral line intensities. National Bureau
    of Standards Monograph 32. 1961.

60. Gaydon, A. G. Dissociation energies and spectra of
    diatomic molecules. Chapman and Hall, Ltd., London,
    England. 1968.

61. Mavrodineanu, R. and H. Boiteux. Flame spectroscopy.
    John Wiley and Sons, Inc. 1965.

62. Molinet, F. Étude de la répartition de la température
    électronique a l'inté rier d'un plasma d'argon produit
    par un générateur h.f. Comptes Rendus de l'Academie
    des Science 262B: 1377. 1966.

63. Johnson, P. D. Temperature and electron density
    measurements in an r.f. discharge in argon. Physics
    Letters 20: 499. 1966.

64. Gol'dfarb, V. M. and S. V. Dresvin. Optical investiga-
    tion of the distribution of temperature and electron
    density in an argon plasma. High Temperature (trans-
    lation of Teplofizika Vysokikh Temperatur) 3: 303.
    1965.

65. American Society for Metals. Metals handbook, properties
    and selection of metals. Vol. 1. 8th edition.
    Novelty, Ohio, American Society for Metals. 1961.

66. Balandin, V. N. and S. L. Mandelshtam. The possiblity
    of a metal composition analysis in an arc furnace without
    sampling (translated title). Zavodskaya Laboratoriya
    23: 545. 1957. Original not available; abstracted in
    Chemical Abstracts 52: 973h. 1958.

67. Shaevich, A. B. and S. B. Shubina. Checking the composition of molten iron without taking a sample. Industrial Laboratory (translation of Zavodskaya Laboratoriya) 28: 469. 1962.

68. Shaevich, A. B., S. I. Melnikov, and V. V. Danilevskaya. On the feasability of monitoring the content of carbon in iron carbide melts by spectroscopic methods without sampling. Industrial Laboratory (translation of Zavodskaya Laboratoriya) 31: 205. 1965.

69. Zipse, E. Analysis of melts, especially steel melts, inside the smelting hearth. West German Patent 1,066,039. Sept. 24, 1959. Abstracted in Chemical Abstracts 55: 13180e. 1961.

70. Nikitina, O. I. and S. D. Gerasimova. Quantitative spectral analysis of melted steel in an electric arc furnace (translated title). Ukrainskii Nauchno-Issledovatel'skii Institut Metallov, Sbornik Trodov, Metallurgizdat No. 8: 361. 1962. Original not available; abstracted in Chemical Abstracts 59: 3312h. 1963.

71. Shaevich, A. B. and S. B. Shubina. [On the spectro-graphic analysis of molten metal without taking a sample.] Konferentsiia po Avtomaticheskomu Kontroliu i Metodam Elektricheskikh Izmerenii, Novosibirsk 1961: 352. 1962.

72. Kustanovich, I. M. Spectrograph for the analysis of molten metals and slag (translated title). Symposium on Materials of the 10th All Union Conference on Spectroscopy, L'vov University, L'vov 2: 451. 1958. Original not available; abstracted in Chemical Abstracts 54: 20363g. 1960.

73. Runge, E. F., R. W. Minck, and F. R. Bryan. Spectro-chemical analysis using a pulsed laser source. Spectrochimica Acta 20: 733. 1964.

74. Hueter, T. F. and R. H. Bolt. Sonics. John Wiley and Sons, Inc., New York, N.Y. 1955.

75. Frederick, J. R. Ultrasonic engineering. John Wiley and Sons, Inc., New York, N.Y. 1965.

76. Carlin, B. Ultrasonics. McGraw-Hill, New York, N.Y.
    1949.

77. ASTM Committee E-2 on Emission Spectroscopy. Methods
    for emission spectrochemical analysis. 4th ed.
    American Society for Testing and Materials. Philadelphia,
    Penna., 1964.

ACKNOWLEDGMENTS